HEALTH AND MEDICINE

Targeted nanoliposomes to improve enzyme replacement therapy of Fabry disease

Judit Tomsen-Melero[1,2], Marc Moltó-Abad[1,3], Josep Merlo-Mas[4], Zamira V. Díaz-Riascos[1,3,5], Edgar Cristóbal-Lecina[1,6], Andreu Soldevila[7], Thomas Altendorfer-Kroath[8], Dganit Danino[9,10], Inbal Ionita[9], Jan Skov Pedersen[11], Lyndsey Snelling[12], Hazel Clay[12]†, Aida Carreño[1,2], José L. Corchero[1,13], Daniel Pulido[1,6], Josefina Casas[6,14], Jaume Veciana[2,1], Simó Schwartz Jr.[1,3,15], Santi Sala[4], Albert Font[7], Thomas Birngruber[8], Miriam Royo[1,6], Alba Córdoba[4]*, Nora Ventosa[2,1]*, Ibane Abasolo[1,3,5,15]*‡, Elisabet González-Mira[2,1]*

The central nervous system represents a major target tissue for therapeutic approach of numerous lysosomal storage disorders. Fabry disease arises from the lack or dysfunction of the lysosomal alpha-galactosidase A (GLA) enzyme, resulting in substrate accumulation and multisystemic clinical manifestations. Current enzyme replacement therapies (ERTs) face limited effectiveness due to poor enzyme biodistribution in target tissues and inability to reach the brain. We present an innovative drug delivery strategy centered on a peptide-targeted nanoliposomal formulation, designated as nanoGLA, engineered to selectively deliver a recombinant human GLA (rhGLA) to target tissues. In a Fabry mouse model, nanoGLA demonstrated improved efficacy, inducing a notable reduction in Gb3 deposits in contrast to non-nanoformulated GLA, even in the brain, highlighting the potential of the nanoGLA to address both systemic and cerebrovascular manifestations of Fabry disease. The EMA has granted the Orphan Drug Designation to this product, underscoring the potential clinical superiority of nanoGLA over authorized ERTs and encouraging to advance it toward clinical translation.

INTRODUCTION

Addressing the therapeutic needs of the central nervous system (CNS) remains a major challenge in the treatment of numerous lysosomal storage disorders (LSDs) and represents an unmet clinical need. Fabry disease (FD: OMIM ID #301500) is one of the most frequent LSD. FD incidence has been estimated at 1:40,000 to 1:117,000 live births (*1*). Mutations in the alpha-galactosidase A (GLA) gene lead to the malfunction or absence of the GLA enzyme and the accumulation of globotriaosylceramide (Gb3) and similar glycosphingolipids in the lysosomes throughout the body, provoking multisystemic clinical manifestations such as progressive kidney disease, cardiac complications, and cerebrovascular disease (*2*). First clinical signs of FD occur during childhood and, over time, microvascular lesions of the affected organs progress, leading to early death. Vasculature is directly involved in the pathophysiology and progression of the FD (*3*, *4*), and thus, endothelial cells are the most predominantly affected cell type in this disease (*5*).

The main treatment option for patients with LSD is the enzyme replacement therapy (ERT), which consists of the intravenous administration of an active recombinant version of the defective enzyme (*5*, *6*). The rationale for ERT is to restore a level of enzymatic activity (EA) sufficient to clear the substrate accumulation in the organ tissues, thereby preventing, stabilizing, or reversing the progressive decline in function of these organs before irreversible damage has occurred (*7*).

For the treatment of FD, two ERTs are authorized in the European Union (EU) since 2001: Replagal (agalsidase alfa) and Fabrazyme (agalsidase beta; also commercialized in United States) (*8*, *9*). However, these treatments offer clinically limited efficacy due to (i) poor biodistribution in target tissues, (ii) inability of recombinant enzymes to cross the blood-brain barrier (BBB), (iii) rapid enzyme degradation and short plasma half-life, and (iv) high immunogenicity (*9*, *10*). Consequently, frequent dosing is required (every other week), resulting in high-cost treatments. To highlight, very recently, a new ERT has been approved by the European Medicine Agency (EMA) and the U.S. Food and Drug Administration, named Elfabrio, which is a novel pegylated, covalently crosslinked form of GLA, which has demonstrated considerable extension of the enzyme's half-life and lower generation of anti-drug antibodies (ADAs) (*11*). However, it has been reported that clinical studies have not established that half-life results in superior efficacy or safety based on clinically relevant end points. The main measure of effectiveness was based on glomerular filtration rate, a measure of how well kidneys

[1]Centro de Investigación Biomédica en Red de Bioingeniería, Biomateriales y Nanomedicina, Instituto de Salud Carlos III, Madrid, Spain. [2]Institut de Ciència de Materials de Barcelona, ICMAB-CSIC, Campus UAB, 08193 Bellaterra, Spain. [3]Clinical Biochemistry, Drug Delivery & Targeting (CB-DDT), Vall d'Hebron Hospital Universitari, Vall d'Hebron Barcelona Hospital Campus, Passeig Vall d'Hebron 119-129, 08035 Barcelona, Spain. [4]Nanomol Technologies SL, Campus de la UAB, 08193 Bellaterra, Spain. [5]Functional Validaton & Preclinical Research (FVPR)/U20 ICTS Nanbiosis, Vall d'Hebron Barcelona Hospital Campus, Passeig Vall d'Hebron 119-129, 08035 Barcelona, Spain. [6]Institut de Química Avançada de Catalunya (IQAC-CSIC), c/ Jordi Girona 18-26, 08034 Barcelona, Spain. [7]Leanbio SL, 08028 Barcelona, Spain. [8]JOANNEUM RESEARCH–Institute for Biomedical Research and Technologies (HEALTH), Neue Stiftingtalstraße 2, 8010 Graz, Austria. [9]Cryo-EM Laboratory of Soft Matter, Faculty of Biotechnology and Food Engineering, Technion-Israel Institute of Technology, 32000 Haifa, Israel. [10]Cryo-EM and Self-Assembly Laboratory, Guangdong-Technion Israel Institute of Technology, Shantou, China. [11]Department of Chemistry and Interdisciplinary Nanoscience Center (iNANO), Aarhus University, DK-8000 Aarhus C, Denmark. [12]Labcorp Drug Development, Harrogate HG3 IPY, UK. [13]Departament de Genètica i de Microbiologia, Institut de Biotecnologia i de Biomedicina (IBB), Universitat Autònoma de Barcelona, 08193 Bellaterra, Spain. [14]Centro de Investigación Biomédica en Red de Enfermedades Hepáticas y Digestivas, Instituto de Salud Carlos III, Madrid, Spain. [15]Servei de Bioquímica, Vall d'Hebron Hospital Universitari, Vall d'Hebron Barcelona Hospital Campus, Passeig Vall d'Hebron 119-129, 08035 Barcelona, Spain.
*Corresponding author. Email: egonzalez@icmab.es (E.G.-M.); ibane.abasolo@vhir.org (I.A.); ventosa@icmab.es (N.V.); acordoba@nanomol-tech.com (A.C.)
†Present address: Altasciences, Office Suire 20, 55 Grove Road, Harrogate HG1 5EP, UK.
‡Present address: Institut de Química Avançada de Catalunya (IQAC-CSIC), c/ Jordi Girona 18-26, 08034 Barcelona, Spain.

are working; supportive data showed a substantial decrease in the levels of Gb3 in the kidneys and blood of patients treated with Elfabrio (ClinicalTrials.gov ID NCT03180840, NCT02795676).

In addition to these ERTs, a pharmacological chaperone therapy, migalastat hydrochloride (Galafold, Amicus Therapeutics UK Ltd), was approved in 2016 only for patients with Fabry disease with amenable GLA mutations (*12*). Migalastat binding stabilizes these mutant forms of GLA in the endoplasmic reticulum and facilitates their proper trafficking to lysosomes (*13*). Once in lysosomes, dissociation of migalastat restores GLA activity, leading to the catabolism of Gb3 and related substrates (*14*). Although migalastat shows several advantages, such as an oral administration, nonimmunogenic response, and potential to cross the BBB, its use is limited to specific FD genetic variants (*15*).

In this context, in the race to develop more effective treatments for FD, several other new strategies are currently under R&D. There are four products in the pipeline, with the majority in phase II, predominantly related to gene therapies: Two of these are adeno-associated virus (AAV) vector variants, e.g., $CD34^+$ hematopoietic stem cell therapy [FLT-190 (ClinicalTrials.gov ID NCT04040049, NCT04455230)] and an AAV2/6 vector-mediated gene transfer [ST920 (ClinicalTrials.gov ID NCT04046224)], and one of these is a lentiviral vector–based therapy [AVR-RD-01 (ClinicalTrials.gov ID NCT03454893)]. In phase III clinical trial, there is the glucosylceramide synthase inhibitor lucerastat (ClinicalTrials.gov ID NCT03425539). Therefore, the FD market is expected to have several novel entrants by 2030 if these aforementioned products, now in clinical phase, succeed. These novel therapies will provide a key opportunity to address the need for long-term highly efficacious therapies. Novel formulations should protect the active biomolecules from degradation, reduce enzyme immunogenicity, enhance enzyme cellular internalization, and improve the treatment efficacy by reaching not only peripheral organs but also the brain (*16*). Accessing the CNS is still one of the main challenges of ERT. Actually, recombinant enzymes infused intravenously fail to cross the BBB and access the CNS (*17*–*19*). This indicates that there is still room to improve ERT formulations for treating FD and other LSD (*20*).

Here, we present a potentially more effective ERT for FD, which is based on a peptide-targeted nanoliposomal formulation that delivers selectively a recombinant human GLA (rhGLA) to endothelial cells. This new liposomal formulation of GLA, named as nanoGLA, has overcome many limitations from the physicochemical point of view, yielding a high-quality liposomal product in line with demanding regulatory requirements. The nanoGLA has demonstrated improved ERT efficacy in preclinical models of FD, inducing a substantial reduction in Gb3 deposits in contrast to non-nanoformulated enzymes, even in the brain. On the basis of the potential clinically relevant advantage of the nanoGLA versus authorized ERTs, such as agalsidase alfa, the EMA has granted nanoGLA the Orphan Drug Designation (*21*). This designation has important implications for the translation of this new therapeutic product from bench to bedside.

RESULTS

Preparation of nanoGLA batches with a specific composition and well-defined production process

New rhGLA and enzyme entrapment into nanoliposomes

In the present work, a new tag-free rhGLA encoded by the GLA gene has been produced using Chinese hamster ovary (CHO) cell culture (CHO K1 cells) following standard cell culture techniques (stable expression-based production method) (*22*) (detailed in Materials and Methods). The rhGLA is a homodimeric enzyme composed of two subunits of 398 amino acids with a monomer weight of 48.8 kDa; the whole GLA has an approximated molecular weight of 100 kDa. Each monomer contains three N-linked glycosylation sites. The amino acid sequence presents 12 cysteines, 10 of which are involved in five disulfide bonds, and therefore, two are free cysteines. Unlike previous reported studies (*23*–*25*), the new rhGLA produced in this work does not contain tags, which reduces the risk of being a highly immunogenic protein (*26*). The amino acid sequence of this rhGLA is identical to the natural GLA, i.e., not chemically modified.

A single 50-liter batch of the new rhGLA was produced and used for the experiments, showing a quality in line with the medicinal product agalsidase beta (Fabrazyme). The latter is used as reference in the quality control of this new rhGLA because both are produced in CHO cells. To note, excipients such as mannitol (30.0 mg ml^{-1}), sodium phosphate monobasic monohydrate (2.75 mg ml^{-1}), and sodium phosphate dibasic heptahydrate (8.0 mg ml^{-1}) (around pH 7) (hereafter named as "rhGLA raw excipients") have been added to stabilize the protein. For the rhGLA batch produced in this work, the physicochemical/biological properties that are critical for recombinant proteins' quality were analyzed and are summarized in Table 1 and fig. S1. The results revealed an identity, potency, structure, and product-related variants consistent with the commercial agalsidase beta product.

The new rhGLA is entrapped through a noncovalent binding into nanoliposomes composed of dipalmitoylphosphatidylcholine (DPPC), cholesterol, and cholesterol–PEG400 (polyethylene glycol, molecular weight 800)–RGD targeting ligand moiety (cyclic-RGDfk, arginine-glycine-aspartic acid) in a molar ratio 10:6.5:0.5, with a small amount of the nonlipid cationic miristalkonium chloride (MKC) surfactant (5 mole % in respect to the other membrane excipients). The resulting nanoformulation has been designated as nanoGLA. Briefly, the nanoGLA is produced in two steps: (i) DELOS (i.e., depressurization of an expanded liquid organic solution) manufacturing process produces an intermediate aqueous dispersion of GLA-loaded nanoliposomes, and (ii) this intermediate dispersion undergoes a tangential flow filtration (TFF) process to concentrate the formulation, diafiltrate, and exchange the dispersant medium and remove the organic solvents and nonintegrated molecules to obtain the final product (fig. S2).

The TFF step allows the concentration of the nanoformulation to increase rhGLA concentration to $\geq$0.2 mg ml^{-1}, to ensure a minimal effective dose to enter in vivo efficacy testing. Previously, a strategy of directly producing liposomes at higher cargo of rhGLA by DELOS has also been explored. However, this option was discarded after observing that the weight ratio between rhGLA and the components forming the nanoliposomal system (i.e., DPPC, cholesterol, cholesterol-PEG400-RGD, and MKC) had a critical impact on the physicochemical properties and stability of the nanoGLA. Batches prepared by DELOS at ratios $\leq$36 μg of GLA per mg of liposomal components presented homogeneous opalescence and maintained stable appearance over time, a mean particle size around 120 to 150 nm and a polydispersity index (PDI) below 0.20 in all cases. On the other hand, batches prepared with higher ratios of GLA to membrane components showed a compromised colloidal stability, leading to aggregation and sedimentation of the liposomal dispersion

just few hours after their preparation, and increase of PDI values in particle size distribution (≥0.40) (fig. S3).

Selection of an optimal isosmotic dispersant medium

The selection of the optimal dispersant medium in which both the nanoliposomes and the enzyme are stable, as well as the suitable pH and osmolality for the intended route of administration (intravenous), is another critical aspect that has been considered. It is well known that parenteral liposomal products should aim toward being isotonic (approximately 280 mOsm kg^{-1}) to prevent rupture or contraction of the liposomal structure and to ensure hemocompatibility.

The osmolality of the nanoGLA has been monitored when pure water is used as dispersant medium during the two steps of the manufacturing route: (i) The intermediate product from the DELOS shows high osmolality (close to 800 mOsm kg^{-1}, being hyperosmotic) due to the presence of traces of both organic solvents used to solubilize the membrane components during the DELOS process, ethanol (EtOH) and dimethyl sulfoxide (DMSO) (fig. S4 and table S1), while (ii) osmolality falls to zero (being hypoosmotic) after the TFF diafiltration process (i.e., after removing the organic solvents used during the DELOS process and nonintegrated molecules such as free GLA), as shown in Fig. 1A. During diafiltration, the osmolality decreases, indicating the successful removal of the organic solvents through the exchange of the initial medium for another, in this case phosphate-buffered saline (PBS) buffer or pure water. These findings highlight the need to explore the addition of more excipients to adjust the nanoformulation osmolality.

To adjust the nanoformulation osmolality, a screening of different isosmotic media suitable for the GLA-loaded liposomes has been carried out. The use of salts composed of ions (e.g., phosphates and sodium), as well as sugars (e.g., sucrose, glucose) and some

Table 1. CQA and specifications of rhGLA. Relevant attributes or CQA of the produced rhGLA and the specifications that must need to ensure the drug substance quality. N/A, not applicable; cIEF, capillary isoelectric focusing; HMW, high–molecular weight; HPLC: high-pressure liquid chromatography; LAL: limulus amebocyte lysate; qPCR: quantitative polymerase chain reaction; RP: reverse phase; SDS-PAGE: SDS–polyacrylamide gel electrophoresis; SEC: size exclusion chromatography; CFU, colony-forming unit.

CQA		rhGLA batch	Specification range for drug substance
Content	Protein concentration	3.11 mg ml^{-1}	N/A
Identity	Immunological detection	Consistent with reference material	Immunoreactive band at 50 kDa (by Western blot)
	Isoelectric point determination	5.11	5.5 ± 0.5 (by cIEF)
Potency	Enzymatic activity	84%	80 to 120% respect to reference material (by fluorescence)
Purity	Electrophoretic pattern	93.14%	>90% (by non-reducing SDS-PAGE)
		91.62%	>90% (by reducing SDS-PAGE)
	HMW variants	85.91%	>85% (by SEC-HPLC)
	C-terminal heterogeneity	94.51% (purity)	>90% (by RP-HPLC)
	Main species	89.94%	
	Species 1	3.29%	
	Species 2	6.77%	
Process related impurities	Microbial contamination	<10 CFU ml^{-1}	<10 CFU ml^{-1} (by bioburden)
	Endotoxins	<80.4 EU mg^{-1}	<100 EU mg^{-1} (by LAL method)

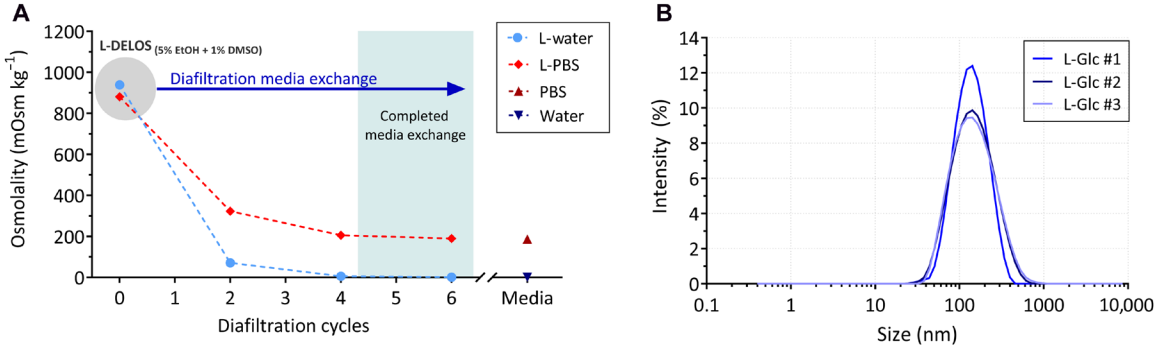

Fig. 1. Impact of the dispersion media on the nanoGLA formulation. (**A**) Evolution of the osmolality of liposomal formulation during buffer exchange by TFF diafiltration, in water (L-water) or in PBS (L-PBS), determined by measurements of the freezing point. Media refers to water and PBS alone. (**B**) GLA-liposomes after TFF concentration and diafiltration in 5% glucose solution (L-Glc). Size distribution of three independent batches.

amino acids, is widely used for osmolality adjustment in liposomal-based nanomedicines approved for the intravenous route (*27*, *28*). Therefore, GLA-loaded liposomes were prepared in water by DELOS, and then, water was exchanged for a set of different isosmotic media in the TFF diafiltration step (schematized in fig. S5A) based on excipients reported in the literature. These media were composed of sugars (glucose, trehalose, and sucrose), in addition to some amino acids (histidine and glycine), salts as sodium chloride, and a mix of sodium phosphates and mannitol, similar to the buffer used with the rhGLA to stabilize the protein (previously introduced as rhGLA raw excipients buffer). The concentration of each media was adjusted to a range of 260 to 300 mOsm kg^{-1} (see table S2).

The results showed the following trend: When sugars or amino acids [such as glucose (Glc), trehalose (Tre), sucrose (Suc), and combinations such as sucrose and glycine (Suc/Gly) or sucrose/histidine (Suc/His)] were used as osmotic agents, the stability and enzyme entrapment efficiency (EE) of the nanoformulation were largely preserved after the diafiltration process; however, when salts were used (e.g., sodium chloride and PBS), the enzyme was markedly released from the nanoliposomes during the diafiltration process, reducing the enzyme EE, as shown in Table 2.

Among nanoformulations with dispersant medium composed of sugars, those containing sucrose and its combination with the amino acids (i.e., Suc/His and Suc/Gly) showed lower colloidal stability, as predicted by the lower ζ-potential values. In addition, the morphology of the nanoliposomes assessed by cryo–transmission electron microscopy (cryo-TEM) (see fig. S6) displayed some changes when sugars were added: In the presence of glucose, nanoliposomes were similar to those detected after diafiltration in water, with a majority of unilamellar vesicles and no presence of aggregates. Conversely, diafiltration with added trehalose induced elongation of some vesicles and an apparent thicker membrane bilayer and in glycine presence nanoliposomes showed a more heterogeneous morphology. GLA-specific EA was maintained when nanoliposomes were diafiltrated in the different isosmotic media, and in all samples, values were comparable to the commercial standard agalsidase alfa, selected as the comparator for preclinical development (fig. S5C). Only liposomes in glycine 2.5% seemed to show a slightly lower biological activity, probably because of the high pH of this media. GLA is a lysosomal enzyme whose optimal working pH is more in the acidic range.

Last, 5% glucose solution was selected as the optimal isosmotic medium for the nanoGLA for the final product because liposomes in this media maintained good physicochemical characteristics, unilamellar morphology, and stability and retained GLA with high entrapment efficiencies and EA (fig. S5, C and D).

Robust manufacturing process: Batch size increase for the first preclinical studies

The manufacturing of the required nanoGLA amount to carry out the first in vivo studies in the preclinical phase, which involve high number of animals, turned out to be a big challenge.

A set of identical batches, with a batch size between 600 and 700 ml, was produced by DELOS up to the required quantity. DELOS is a robust and green nanoformulation production platform based on compressed carbon dioxide (CO_2). Briefly, the process

Table 2. Summary of physicochemical characterization of GLA-liposomes (L) diafiltrated in different isosmotic media at time 1 day after production or, in parenthesis, 2 weeks after production. Details of the media composition are shown in table S2. Glc, glucose; Tre, trehalose; Suc, sucrose; His, histidine; Gly, glycine; NaCl, sodium chloride; Exc, mixture of excipients (mannitol, sodium phosphate monobasic monohydrated, sodium phosphate dibasic heptahydrated. Average of two independent batches.

Diafiltration media	Size* (nm)	PDI†	ζ-pot‡ (mV)	GLA§ (μg ml^{-1})	EE (%)¶	Osmolality (mOsm kg^{-1})
L-DELOS	121 ± 2 (125 ± 5)#	0.26 ± 0.02 (0.27 ± 0.01)#	61 ± 1 (56 ± 1)	21 ± 1	–	1049 ± 10
L-Water	138 ± 3 (134 ± 7)	0.29 ± 0.02 (0.26 ± 0.01)	41 ± 8 (35 ± 4)	19.6 ± 0.4	92 ± 7	0 ± 2
L-Glc	113 ± 4 (110 ± 3)	0.21 ± 0.01 (0.20 ± 0.01)	47 ± 1 (49 ± 3)	21 ± 1	99 ± 9	294 ± 5
L-Tre	120 ± 1 (122 ± 1)	0.25 ± 0.01 (0.23 ± 0.01)	38 ± 1 (35 ± 5)	17.8 ± 0.2	84 ± 5	324 ± 23
L-Suc	132 ± 8 (148 ± 14)**	0.23 ± 0.01 (0.25 ± 0.02)**	29 ± 2 (22 ± 4)	19 ± 2	90 ± 14	284 ± 4
L-Suc/His	232 ± 2** (300 ± 15)††	0.43 ± 0.06** (0.49 ± 0.06)††	15 ± 2 (14 ± 1)	23.1 ± 0.2	100 ± 10	291 ± 5
L-Suc/Gly	143 ± 3 (174 ± 1)**	0.24 ± 0.01 (0.25 ± 0.02)**	26 ± 3 (30 ± 2)	17.1 ± 0.1	87 ± 2	282 ± 5
L-Gly	128 ± 1 (124 ± 1)	0.26 ± 0.01 (0.23 ± 0.01)	35 ± 1 (35 ± 2)	21.6 ± 0.6	110 ± 6	297 ± 5
L-NaCl	125 ± 1 (134 ± 1)††	0.25 ± 0.01 (0.41 ± 0.03)††	6 ± 1 (7 ± 1)	<LOD	0	256 ± 5
L-Exc	125 ± 1 (123 ± 1)	0.19 ± 0.01 (0.20 ± 0.01)	13 ± 1 (14 ± 1)	<LOD	0	275 ± 5

*Liposome diameter. †Polydispersity index. ‡ζ-potential. §GLA concentration in the formulation. ¶GLA entrapment efficacy. #Some sediment but resuspended well. **Milky appearance. ††Milky appearance and some sedimentation.

consists of the addition of liquid compressed CO_2 into an organic solution containing all membrane components, followed by the depressurization of the CO_2-expanded solution into an aqueous solution containing the rhGLA, resulting in the formation by self-assembly of the nanoGLA liposomes dispersed in water with small amount of organic solvent (around 5% volume). All produced batches showed an extreme robustness of the DELOS process. The coefficient of variation (CV) was ≤10% in several parameters such as size (CV, 7%; $n = 6$), PDI (CV, 10%; $n = 6$), and ζ-potential (CV, 7%; $n = 6$). This low batch to batch variability in the production method is a very important milestone for translation of nanomedicines from the bench to bedside.

Next, individual batches were mixed in a pool, obtaining up to 3.5 liter of intermediate nanoGLA. This represented an increase in batch size over the initial production capacity of the system (*24*, *25*). Intermediate nanoGLA was then submitted to a TFF process, consisting in a 7.5-fold concentration followed by a diafiltration step to substitute the initial dispersion media [water with 5% (v/v) of organic solvent] for a glucose solution [5% (w/v)] and to remove non-incorporated compounds, obtaining the final nanoGLA.

Quality assessment, specifications, and complementary characterization

Before initiating in vivo studies, the nanomedicine candidates were characterized by using robust, straightforward, and affordable methods, to ensure the production of a high-quality product, and control of the physicochemical/biological properties that influence efficacy and safety. The accurate identification of critical quality attributes (CQAs) for both the drug substance and the resulting drug product remains a crucial step in the quality and safety assessment of nanomedicines under development. The identification of the CQAs and control strategies to ensure that these CQAs are within an appropriate limit, range, or distribution (i.e., specifications) to guarantee the desired product quality was preliminary performed and reported by Merlo-Mas *et al.* (*25*).

For the nanoGLA batches produced in this work (nanoGLA#1 and nanoGLA#2), the physicochemical/biological properties that are critical for product quality were characterized and summarized in Table 3. Notably, the intermediate products immediately after DELOS (without any post-processing such as TFF) were also characterized to ensure the quality of both in-process and final products.

The morphology of the systems was studied using cryo-TEM after sample vitrification. This methodology allows direct investigation of colloidal systems, such as liposomes, in the hydrated state, so their structure is well preserved close to the native state. Cryo-TEM analyses have depicted that these nanoformulations were uniform, and vesicles were spherical and mostly unilamellar, with diameters ranging between 50 and 300 nm (see Fig. 2A). Therefore, this CQA was within specifications as well. GLA was visible interacting with the vesicles (arrows).

The cross-section structure of the bilayers, the lamellarity of the nanovesicles, and the concentration of the GLA in the nanoformulations were further determined by small-angle x-ray scattering (SAXS) in a similar way as done previously (*24*, *25*). The data were analyzed by a model where the cross section of the membrane is described by three Gaussian functions of fixed width, where the central Gaussian describes the low-electron density hydrocarbon region, and the two outer ones describe the head groups and RGD. The central Gaussian has a fixed scale factor of −1, and the scale of the head boxes is optimized in the fit. The width of the bilayer is given by the full width half-maximum value of the profile. The multilamellarity was described by

Table 3. CQA and specifications of nanoGLA. Relevant attributes or CQAs of the nanoGLA, and the specifications that must meet to ensure the product quality. DLS, dynamic light scattering. ELS, electrophoretic light scattering; UV, ultraviolet.

		nanoGLA #1 batch		nanoGLA #2 batch	
CQAs	**Specification range for final product**	**Intermediate product (in process control)**	**Final product**	**Intermediate product (in process control)**	**Final product**
Appearance	Homogeneous aqueous dispersion without sediment and opalescent appearance macroscopically	Homogeneous whitish aqueous dispersion without sediment and opalescent appearance macroscopically	Homogeneous whitish aqueous dispersion without sediment and opalescent appearance macroscopically	Homogeneous whitish aqueous dispersion without sediment and opalescent appearance macroscopically	Homogeneous whitish aqueous dispersion without sediment and opalescent appearance macroscopically
Particle size	50–300 nm (by DLS)	151 ± 1 nm	124 ± 1 nm	176.3 ± 0.2 nm	153 ± 1 nm
Polydispersity index	≤0.45 (by DLS)	0.16 ± 0.01	0.13 ± 0.01	0.20 ± 0.01	0.09 ± 0.02
***Z* potential**	>+20 mV (by ELS)	41 ± 1 mV	45 ± 2 mV	39 ± 2 mV	40 ± 1 mV
Potency-specific EA	Bioactive (ratio of nanoGLA versus freeGLA ≥0.50)	Bioactive (0.92 ± 0.05)	Bioactive (0.65 ± 0.02)	Bioactive (0.84 ± 0.01)	Bioactive (0.63 ± 0.02)
Total GLA content	≥30 μg ml^{-1} (for intermediate)/≥200 μg ml^{-1} (for final product) (by RP-HPLC-UV)	27 ± 1 μg ml^{-1}	216 ± 10 μg ml^{-1}	37 ± 2 μg ml^{-1}	270.90 ± 0.04 μg ml^{-1}
pH	6.0–7.0 (for final product)	5.2 ± 0.2	6.27 ± 0.08	5.5 ± 0.2	7.04 ± 0.04
Osmolality	260–300 mOsm kg^{-1} (for final product)	936 ± 5 mOsm kg^{-1}	291 ± 5 mOsm kg^{-1}	932 ± 5 mOsm kg^{-1}	265 ± 5 mOsm kg^{-1}

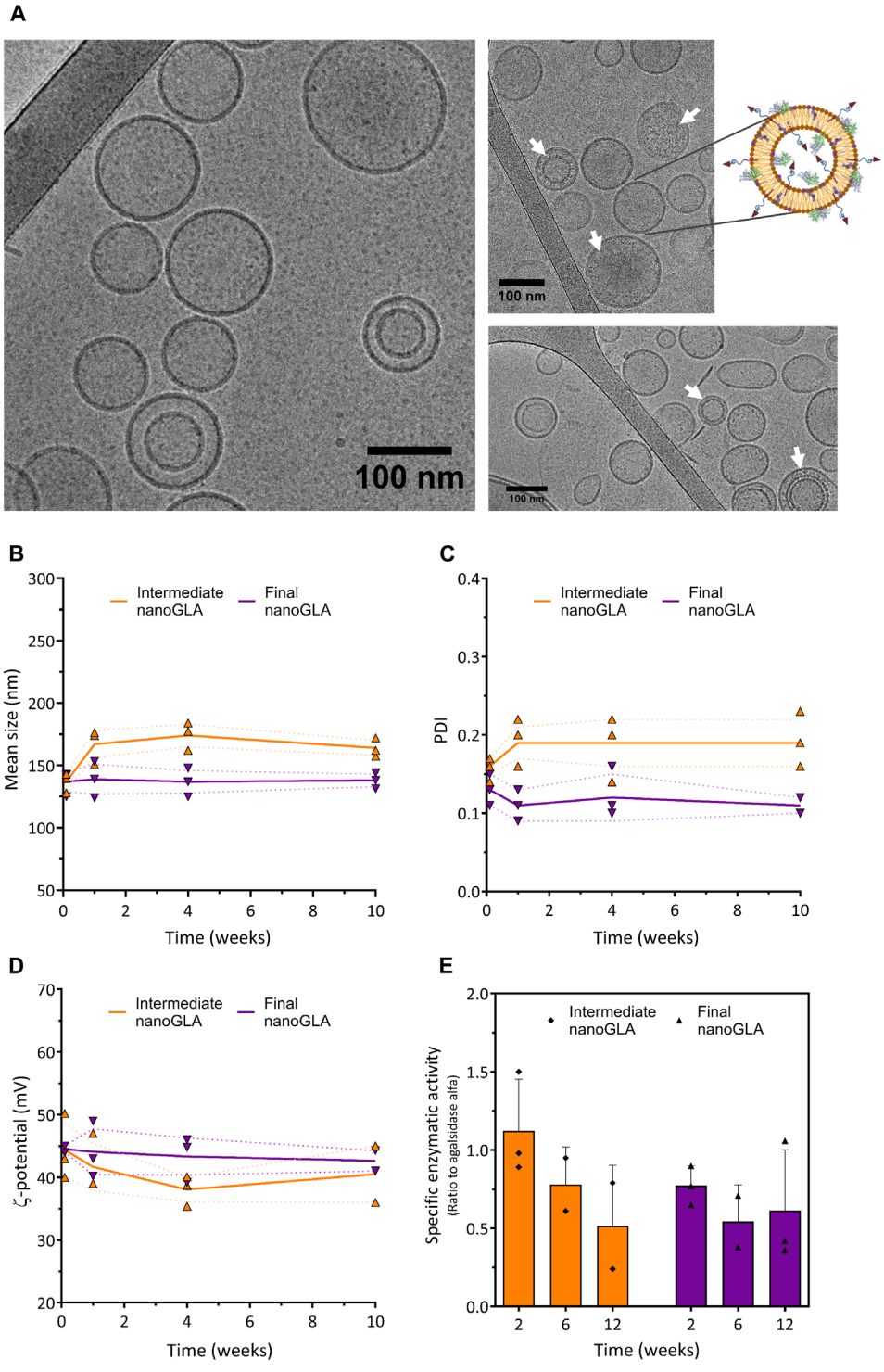

Fig. 2. Morphology and stability of nanoGLA. (**A**) Morphology of nanoGLA, analyzed by cryo-TEM, 1-week after production. White arrows highlight interactions between the enzyme and the nanoliposome. (**B** to **E**) Stability of nanoGLA stored at 2° to 8°C in terms of: (B) size, (C) PDI, (D) ζ-potential for 10 weeks. For each system, three independent batches per time point are represented (symbols) and the average (continuous line; SD represented by dotted lines). (E) Stability of specific enzymatic activity (EA) for 12 weeks, average of three independent batches. Values expressed in relation to reference GLA (agalsidase alfa).

a para-crystal model, where only one and two membranes are included. The spacing between the layers is described by *D*, and the disorder of this distance is described by σ_{disord} and is a fraction of *D*. The fraction of single layers was also calculated and is given in table S3. The concentration GLA was determined as the scale factor of a contribution to the scattering measured separately for a pure GLA solution. All these parameters were calculated for intermediate and final nanoGLA, as detailed in table S3. The modeling provided good fits to the data as reflected by the reduced χ^2 values (goodness of fit) in table S3, although it is somewhat higher for the high-concentration sample due to the better counting statistics for this sample. The model gives similar cross-section profiles with a nearly constant bilayer width of 50 to 52 Å and a low degree of multilamellarity.

The GLA concentration in the nanoGLA formulations could be also estimated by having the SAXS curve for a GLA dimer as a background component. The protein concentration estimations from the SAXS data (table S3) are in very good agreement with the values obtained by reversed phase high-pressure liquid chromatography (RP-HPLC) (Table 3).

The stability of rhGLA drug substance was tested by RP-HPLC, size exclusion chromatography HPLC (SEC-HPLC), and EA after being stored at −80°C for 7 months. The C-terminal variability by RP-HPLC showed consistency after 7-month storage (purity of 92.79%, main species = 89.63%; species 1 = 3.82%; species 2 = 6.55%), indicating no changes in protein integrity. The appearance of new molecular weight variants by SEC-HPLC, related to protein stability during course study, was not detected (main peak = 90.67%). Regarding the EA, no major changes were observed related to the storage at −80°C after 7 months.

The colloidal stability of the nanoGLA formulation, as an aqueous dispersion of nanoliposomes containing the rhGLA, was monitored for 10 weeks. The formulation was stable for at least 2 months (Fig. 2, B to D), indicating that the product development was mature enough to carry out longer studies, e.g., repeated-dose efficacy studies, since the drug product stability covers the period time required for these studies. Regarding EA, GLA in the final nanoGLA liposomes retained its bioactivity for at least 2 months (Fig. 2E).

Advanced preclinical evaluation of nanoGLA for FD treatment

Hemocompatibility

Because the nanoGLA was designed to be administered intravenously, hemocompatibility of the formulation was tested before in vivo assays. In detail, nanoGLA has shown to be nonhemolytic in a hemolysis test using mouse red blood cells (RBCs). Hemolysis values did not surpass 5% of total hemolysis to be considered hemolytic in any of the tested concentrations (fig. S7). In addition, no substantial variations in plasma coagulation times were detected after incubation of plasma with nanoGLA (table S4). In this case, assays were conducted using human plasma from volunteers, which was incubated with liposome dispersion (0.1 mg ml^{-1}). None of the three tested coagulation times—activated partial thromboplastin time (APTT), prothrombin time (PT), and thrombin time (TT)—showed any important alteration when compared to the controls, nontreated plasma and vehicle-treated (PBS) plasma. Thus, nanoGLA was shown to be safe for intravenous administration because no hemolysis signs or alterations in plasma coagulation times were found.

In vitro efficacy

The ability of the nanoGLA to reduce (hydrolyze) the Gb3 substrate was measured by using a fluorescent-labeled Gb3 [nitrobenzoxadiazole (NBD)–Gb3] substrate in mouse aortic endothelial cell (MAEC) derived from Fabry knockout (KO) mice, as previously described (*23*, *24*, *29*). This in vitro assay measures the ability of the enzyme to reach the lysosomes and hydrolyze the substrate of the GLA enzyme, offering a rapid and clear assay to test both the internalization and the efficacy of the tested samples. The nanoGLA prototypes (both intermediate and final products) showed better efficacy than free GLA, with a 50% increased activity over agalsidase alfa at enzyme concentration (0.25 μg ml^{-1}) (see Fig. 3). Conversely, the control nanoformulation without rhGLA (named "empty liposomes" in Fig. 3) showed no substantial activity. The formulation of the rhGLA in nanoGLA notably increases the ability of the enzyme to hydrolyze the Gb3 substrate.

Pharmacokinetic studies in rats

According to the International Council for Harmonisation of Technical Requirements for Pharmaceuticals for Human Use (ICH) S6R1 (*30*), which provides guidance on preclinical safety evaluation of biotechnology-derived pharmaceuticals, information on tissue distribution, disposition, and clearance in relevant animal models should be evaluated. This is essential to assess the pharmacokinetic (PK) properties of the pharmaceutical candidate and its potential effects on various tissues and organs. Therefore, this novel nanoliposomal formulation with promising physicochemical and in vitro biological properties was characterized with respect to PKs to confirm increased half-life of GLA when administered in the nanoliposomes. The rat was the species of choice because the higher blood distribution volume in these animals ensures better PK profiling compared to mice.

PK profile of the unloaded nanoliposomes. A preliminary PK study was carried out, following intravenous administration of the unloaded nanoformulation (without the rhGLA enzyme) to healthy

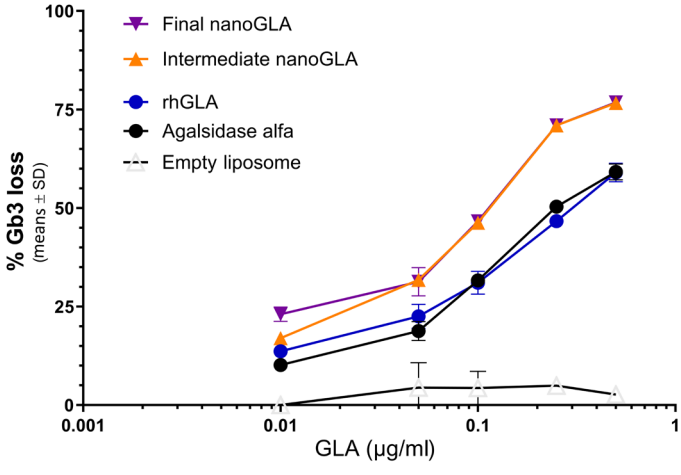

Fig. 3. In vitro efficacy in primary cultures of FD model. Gb3 reduction of the nanoGLA in comparison with the free rhGLA, and the free agalsidase alfa in primary endothelial cells derived from Fabry KO mice. Incubation of GLA (0.25 μg ml^{-1}) (or at the equivalent liposome concentration for empty liposomes) at 37°C for 48 hours. Empty liposomes refer to the nanoformulation without GLA (at the equivalent concentration), used as control. The assay corresponds to a single representative experiment, replicated in three independent assays.

Sprague-Dawley rats. Although the rhGLA enzyme is the drug substance that must be measured to determine the PK profile, we wanted to explore the way to track also the nanocarrier (i.e., the nanoliposomes that contain the rhGLA) in vivo. Accordingly, in this study, we explored the potential of using the MKC surfactant, which is a component of the liposomes but is not naturally present in the body, as a surrogate of the nanoliposomes for in vivo monitoring. The absence of a basal level of this molecule makes it virtually ideal for tracking liposomes in biological matrices. A free MKC group was used as a control (i.e., MKC aqueous solution).

To confirm the suitability of the strategy of using MKC for nanoliposomes tracking, empty liposomes were prepared as described for nanoGLA, but skipping the rhGLA addition step. Empty liposomes showed very narrow vesicle size distribution in the nanometric range, as well as spherical and mostly unilamellar morphology (fig. S8).

Wild-type (WT) rats were assigned to two groups ($n = 6$ male rats per group) and were dosed either with concentrated empty liposomes at liposomes of 30 mg kg^{-1} (equivalent to MKC of 1 mg kg^{-1}) or with free MKC at an equivalent concentration. Blood samples were collected at different time points over the course of 98 min, and plasma MKC concentration was quantified by a liquid chromatography–mass spectrometry LC-MS (see Materials and Methods). Our results indicate that the PK profile of the MKC-containing nanoliposomes is completely different from the free MKC (Fig. 4). The nanoliposomes group showed a total plasma half-life ($t_{1/2}$) of 98 min ($t_{1/2,distribution} = 3$ min, $t_{1/2,elimination} = 95$ min), while free MKC $t_{1/2}$ was <5 min.

This different PK profile was expected since MKC, as free compound, at 0.30 mg ml^{-1} (equivalent to MKC concentration in the liposomal sample) is below the critical micelle concentration (CMC), which is approximately 2.16 mM (0.79 mg ml^{-1}) at 25°C. In the case of the free MKC in solution, before IV bolus administration to rats the MKC concentration was below the CMC, thus as dissolved monomers. In addition, later dilution in the blood stream accentuates this dilution effect. It is known that small molecules, such as the hydrophilic MKC, can be rapidly removed from the circulation after renal or hepatic excretion (*31*, *32*). In contrast, MKC contained in the nanoliposomes showed higher plasma half-life, suggesting that MKC is retained in the nanoliposomes traveling together and, thus, preserving its integrity.

PK profile of the nanoGLA. The aim of this study was to compare the PK of nanoGLA and free rhGLA following intravenous administration to healthy Sprague-Dawley rats ($n = 3$ male rats per group). A bolus dose of nanoGLA [GLA (1 mg kg^{-1})] or the free rhGLA was injected intravenously, and blood samples were collected at different time points over the course of 8 hours to measure the plasma concentration of the total GLA enzyme (Fig. 5 and table S5). The nanoformulated GLA showed a different PK profile, with a higher volume of distribution (0.18 liter kg^{-1} for nanoGLA versus 0.037 liter kg^{-1} for the free rhGLA) and comparable clearance (2.35 ml min^{-1} kg^{-1} for nanoGLA versus 1.8 ml min^{-1} kg^{-1} for the free rhGLA). This is translated into an extended half-life of the GLA when nanoformulated compared to the free rhGLA enzyme (1.8 hours versus 1.1 hours). Average concentration values for total GLA were measurable through 8-hour post-dosed the nanoGLA, as shown in Fig. 5.

Biodistribution of nanoGLA's EA in Fabry mouse model

Enzyme biodistribution after intravenous administration of 1 mg kg^{-1} of the liposomal product, agalsidase alfa, or the free rhGLA was studied in Fabry mice. These are KO animals for the GLA enzyme (*33*), and thus, all the GLA EA found in these animals corresponds to the exogenously administered recombinant enzyme. EA was assessed in plasma and organ tissues 30 min after administration and referred to the activity found in plasma 1 min after administration to better normalize to the administered EA ($n = 4$ per time point). The results showed that animals treated with the nanoGLA had significantly higher levels of EA in plasma compared to the free enzymes (commercialized agalsidase alfa or rhGLA) (Fig. 6). The percentage of EA in plasma was 18.9 ± 0.7% when the rhGLA was nanoformulated in the novel nanoliposomes, and only 2.9 ± 0.2% of EA was measured in the case of free enzymes ($P = 0.024$). Therefore, the nanoGLA protects and prolongs the EA of the active principle (rhGLA) in bloodstream.

The same EA analysis was then performed in the organ tissues to confirm the improved uptake of GLA in these target tissues (Fig. 6). The biodistribution based on EA showed that nanoformulated rhGLA and the free enzymes were mainly retained by the liver (~40 to 80%

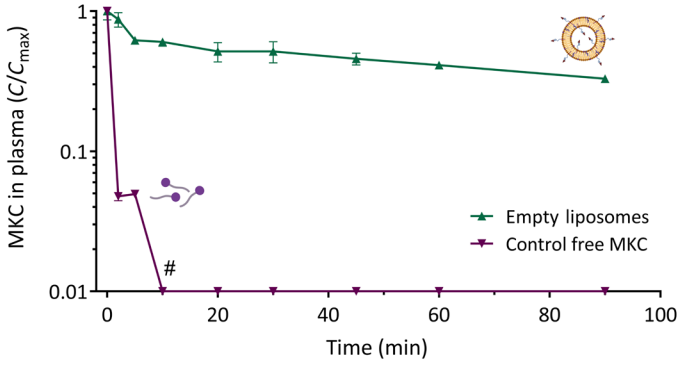

Fig. 4. PK profile of empty liposomes. PK of MKC-containing nanoliposomes versus free MKC ($n = 6$ animals per group, values correspond to the means ± SEM). Both curves have been normalized to the maximum concentration (C_{max}) for better comparison. # denotes values below the limit of detection.

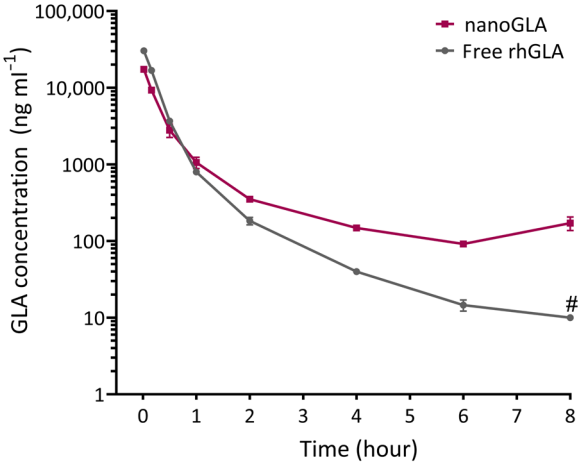

Fig. 5. PK profile of nanoGLA. Mean (± SEM) concentration of total rhGLA in male rat plasma following a single intravenous administration of free rhGLA or nanoGLA (GLA dosing of 1 mg kg^{-1}) ($n = 3$ animals per group). # denotes value below the limit of quantification.

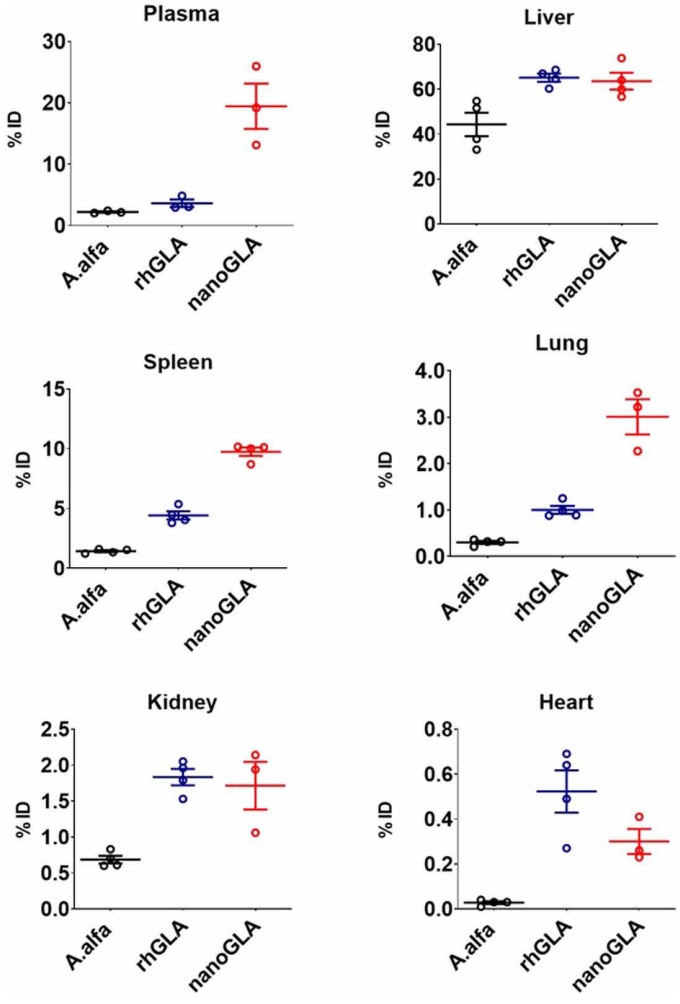

Fig. 6. GLA EA in Fabry mice 30 min after administration. Animals (n = 8 per group) received intravenous nanoGLA, rhGLA or agalsidase alfa (A.alfa) (1 mg kg^{-1}). Activity was measured in plasma and tissues 30 min after administration (n = 4) and referred to activity at 1 min (n = 4). Values in the y axis correspond to the % of injected dose (% ID) and are expressed as the means ± SEM.

EA) and the spleen (1.5 to 13% EA), as shown in Fig. 6. At 30 min after administration, EA retention was higher for rhGLA and nanoGLA compared to agalsidase alfa in the liver and spleen (P = 0.0012 and P = 0.0017, respectively). In addition, nanoGLA had a higher accumulation in the spleen and lung compared to free GLA (P < 0.0001 and P = 0.0001, respectively).

NanoGLA reached the kidney and heart, two of the target organs for FD ERT, in a greater extent than the commercially available enzyme (agalsidase alfa), with statistical P values being 0.0061 and 0.0389, respectively. No significant differences were observed between rhGLA and nanoGLA in terms of EA in these two organs (Fig. 6). Differences between the rhGLA and the agalsidase alfa might be due to the different cell source, resulting in enzymes with different patterns of glycosylation; rhGLA, as agalsidase beta, is obtained in CHO cells, whereas agalsidase alfa is obtained in cells of human origin. Compared to agalsidase alfa, agalsidase beta has higher levels of mannose-6-phosphate and higher kidney accumulation (*34*). However, the superior cardiac and renal accumulation of rhGLA versus agalsidase alfa might be also due to an improved GLA production method because alternative versions of human recombinant GLA enzyme obtained from CHO cells have rendered lower enzymatic activities in the kidney than aglasidase-beta (*29*).

Efficacy studies in Fabry mouse model

The in vivo efficacy of the nanoGLA, as an alternative to the conventional ERT therapy, was tested in the Fabry KO mice. The Fabry KO mice model (GlatmKul in C57BL6 background) is the most widespread animal model for FD and has a complete absence of the GLA gene (*33*). These mice exhibit typical lipid inclusions with lamellar structures in the lysosomes and progressive accumulation of Gb3 in target tissues, including the heart and kidneys, following the same pattern as in the human patients with Fabry disease. Thus, for determining the in vivo efficacy of nanoformulated GLA, Fabry mice were treated with a single intravenous administration of nanoGLA, free (nonentrapped) rhGLA, or the clinically available agalsidase alfa (free enzyme as well) at the dose of 1 mg kg^{-1} (n = 8 animals per group). For the repeated-dose efficacy assay, animals received eight doses of the test compounds. In the absence of any record of side-effect or weight loss in the animals, we concluded that the treatment was well-tolerated in the tested dose range. One week after the last administration (for single dose) or 24 hours after the last administration (for repeated dose), mice were euthanized and Gb3 levels in the different organs (liver, spleen, kidney, heart, lung, and brain) were determined by LC in tandem with high-resolution MS (LC-HRMS) (see Materials and Methods).

Absolute Gb3 levels in picomole equivalent per milligram of protein of animals treated with a single dose are shown in table S6. For clarity, Gb3 levels are presented in Fig. 7 as Gb3 loss (%), showing the basal situation of WT animals with the 100% of Gb3 loss compared to that of nontreated KO mice with a 0% of Gb3 loss. In between, GLA-treated animals showed a variable response, but in all organs analyzed, except the liver, Gb3 loss is higher in the nanoGLA-treated group than in the agalsidase alfa or rhGLA-treated groups (Fig. 7A). In the liver, where large amounts of GLA are delivered after systemic administration (see previous biodistribution results), Gb3 reduction in GLA-treated groups is close to the expected values in WT animals, and differences between treatments are minimal. In other organs receiving lower amounts of enzyme, nanoGLA showed a greater ability to reduce the Gb3 deposits than rhGLA or agalsidase alfa. Specifically, in the kidney and heart, two of the organs most affected by FD, nanoGLA showed greater efficacy compared to the rhGLA or agalsidase alfa (Fig. 7A; P = 0.0166 and P = 0.0035 in the kidney and heart, when comparing with rhGLA). These results are consistent with a higher volume of distribution found in the PK study for the nanoGLA formulation and superior distribution found in the mentioned tissues.

Having demonstrated the ability of nanoGLA to reduce Gb3 levels after a single intravenous administration, a repeated-dose efficacy study was conducted. The results obtained showed that, after eight administrations of 1 mg kg^{-1} equivalent of enzyme to Fabry KO mice (n = 6 animals per group, receiving intravenous administrations every other day), nanoGLA induced a higher and significant loss of Gb3 in plasma and all tissues tested (liver, spleen, lung, kidney, heart, and brain) compared to the free enzymes (see Fig. 7, B and C; P values being 0.0043 and 0.0095 in the kidney and heart, when compared to the agalsidase alfa). Furthermore, in the kidney, the Gb3 loss induced by repeated nanoGLA administration was more significant than that observed with single dosing

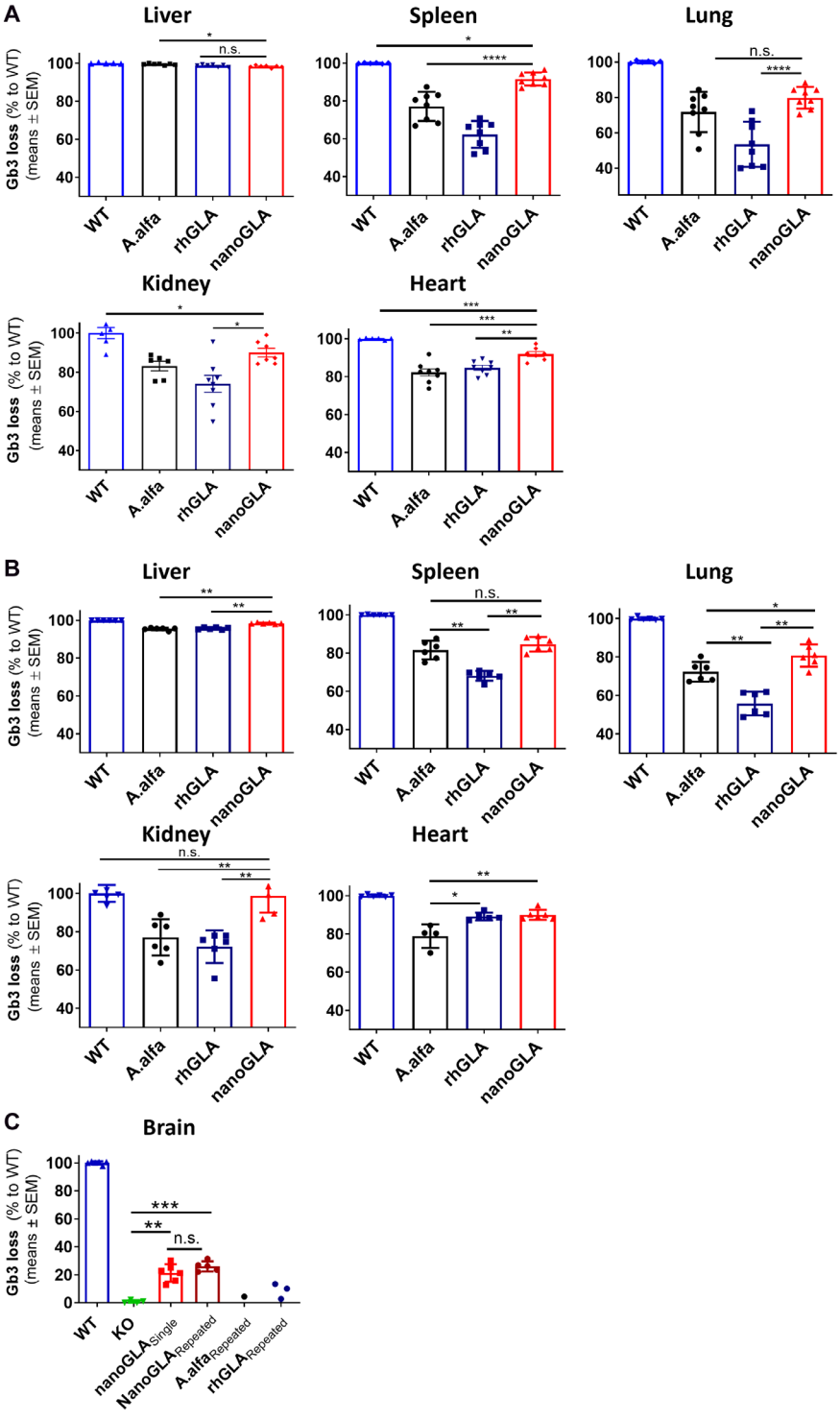

Fig. 7. In vivo efficacy of nanoGLA in Fabry mice. (**A**) Loss of Gb3 in Fabry mice with single intravenous administration of nanoGLA, free rhGLA, and free agalsidase alfa (A.alfa) ($n = 8$ animals per group). (**B**) Loss of Gb3 in Fabry mice receiving eight doses (every other day) of the same treatments ($n = 6$ animals per group. All administration were at 1 mg of GLA kg^{-1} dose. WT animals are included as controls (100% of Gb3 loss). (**C**) Comparative efficacy of the nanoGLA treatment in the brain of Fabry mice after a single or repeated dosing, as percentage of Gb3 loss. Results are compared with the nontreated WT and KO animals, as well as with the efficacy of the free non-nanoformulated enzymes (rhGLA and A.alfa) after repeated dosing. Analysis of variance (ANOVA) test and Tukey's multiple comparison test were performed to compare results. Statistical differences that are not obvious and are relevant for understanding the behavior of nanoGLA are shown [n.s. (nonsignificant), $P \leq 0.05$; $^{**}P \leq 0.01$, $^{***}P \leq 0.001$, or $^{****}P \leq 0.0001$].

(see absolute Gb3 values in tables S6 and S7, corresponding to 4557 ± 860 and 8339 ± 689 pmol eq/mg of protein in the kidneys of repeated and single-dose administration groups, respectively, with a *P* value of 0.0024), indicating that the efficacy already observed after a single-dose administration can be improved by subsequent dosing.

Repeated dose of nanoGLA also induced a reduction of Gb3 levels in brain (Fig. 7C). The efficacy of repeated-dose nanoGLA in the brain (approximately 28%) was higher than that observed with a single dose (ca. 21%), although these differences were not significant (see Fig. 7C). This reduction in Gb3 levels in brain when mice were treated with single or repeated dose of nanoGLA was not seen with any of the free non-nanoformulated enzymes (neither the free rhGLA nor the commercial agalsidase alfa). This is an interesting finding as it suggests that, unlike any of the currently approved recombinant enzymes for ERT, nanoGLA is able to cross the BBB and reduce the Gb3 deposits in the brain parenchyma.

DISCUSSION

The current work presents a comprehensive optimization process of the GLA-loaded RGD-targeted nanoliposomes formulation, designated as nanoGLA and developed as potential advanced therapy for FD to target systemic and cerebrovascular manifestations. CQAs for nanoGLA were accurately defined, encompassing both physicochemical and biological properties crucial for ensuring product quality. Furthermore, these established CQAs were validated by the EMA through a scientific advice procedure.

Unlike the GLA model used in previous studies (*24*, *25*), these nanoliposomes were loaded with a new tag-free rhGLA with the potential for further advancement in pharmaceutical development. This advancement contributed to enhance the quality of the nanoGLA formulation, meeting all established CQA criteria. Besides, successful scaled-up production of nanoGLA was achieved, providing the required quantity and quality for preclinical testing. It was possible to first scale up the nanoGLA production from 25 ml to volumes ranging between 150 and 900 ml per batch using the DELOS process. DELOS is a robust and eco-friendly technology for the manufacturing of nanomedicines, including liposomes and other colloidal systems, which offers a high control over particle properties. It enables to nanoformulate a large variety of drug modalities, from small chemical molecules to peptides, proteins, and nucleic acids (*25*, *35*, *36*). The process is based on the use of compressed CO_2, is scalable, and is compliant with the Good Manufacturing Practice requirements. The nanoGLA production scale up demonstrated a notable flexibility in terms of batch size, reinforcing the suitability of the DELOS for the consistent preparation of nanoconjugates. This reliable batch-to-batch reproducibility represents an important milestone for the successful translation of nanomedicines from the bench to the bedside. To achieve the required GLA concentration in the nanoGLA formulation, an additional diafiltration/concentration step through a TFF procedure was implemented to enable in vivo dosing at therapeutic levels (1 mg kg^{-1}). This dosage was selected after a comprehensive review of previous preclinical studies assessing GLA's efficacy in Gb3 clearance assays, where doses ranging from 1 to 3 mg kg^{-1} were consistently effective after single-dose or repeated administrations (*37*–*42*).

Another pivotal consideration was the selection of an optimal nanoliposomal dispersant medium for the intended administration route (intravenous), ensuring stability of the nanoliposomes and enzyme, as well as appropriate pH and osmolality to prevent nanovesicle structural compromise and guarantee hemocompatibility. Initial osmolality assessments of the nanoGLA prototype highlighted the necessity of the use of isosmotic agents to adjust it, as nanoformulations deviated notably from blood osmolality, a key parameter for intravenous administration. Osmolality measurements of the samples just after DELOS production revealed hyperosmotic conditions attributed to traces of the organic solvents used during component solubilization in the manufacturing process. While the clinical field well knows this effect and the measurement of the serum osmolality is used to determine the presence of a possible toxic alcohol ingestion or evidences for other certain types of diseases (e.g., dehydration or hyperglycemia) (*43*–*45*), its consideration in formulation development when organic solvents are used is little reported. Here, osmolality measurements facilitated indirect estimation and control of residual organic solvents in the nanoformulation.

Reviewing literature on marketed liposomal-based nanomedicines approved for intravenous administration revealed different approaches to osmolality adjustment, including not only the use of salts composed by small ions (e.g., phosphates and sodium), which are the most broadly used, but also the use of sugars and amino acids. Notably, details concerning media incompatibilities are typically outlined in the information leaflet for several marketed liposomal-based nanomedicines. For instance, AmBisome explicitly advises against reconstitution with saline, specifying dilution only with 5% dextrose solution to prevent precipitation saline (*46*). Similar directives are found for other liposomal drugs such as DaunoXome, Doxil, Caelyx, or Visudyne, emphasizing meticulous media selection to preserve formulation integrity (*47*–*50*). This screening was crucial in nanoGLA development, where testing different isosmotic media revealed substantial impacts on enzyme EE. The use of PBS, for instance, resulted in GLA leakage due to a reduction of the electrostatic interaction of the enzyme with the liposomal membrane, resulting in the need of alternative isosmotic media exploration. Optimal results were achieved with 5% glucose solution, which was selected as the isosmotic dispersant medium for nanoGLA.

Furthermore, new analytical methodologies were implemented, including an RP-HPLC method for GLA quantification and an LC-MS method for determining MKC concentration in biological samples. The tracking of the MKC from nanoliposomes in plasma showed extended circulation half-life of this liposomal membrane component compared to the free MKC surfactant used as control. This different PK profile of the MKC surfactant indirectly confirmed the sustained presence of these nanoliposomes in blood circulation, preserving their integrity.

Overall, we achieved successful optimization of the nanoGLA, enabling its progression to an advanced stage of preclinical development. Efficacy studies in a murine model of FD, involving both single- and repeated-dose administrations, demonstrated increased GLA activity in plasma and enhanced Gb3 clearance in the liver, spleen, lung, heart, kidney, and even in the brain parenchyma compared to non-nanoformulated enzymes (including the commercially available agalsidase alfa, Replagal). These findings were consistent with the extended plasma half-life observed in a PK study in rats when compared with the free rhGLA enzyme.

In patients with Fabry disease, the accumulation of Gb3 in the kidneys can begin as early as 17 weeks of gestation, progressing gradually and correlating directly with early renal damage and albuminuria (*51*). The Gb3 accumulation in kidney cells and consequently podocyte loss in urine precedes clinical manifestations (i.e., proteinuria), meaning that the cellular damage occurs before tissue damage becomes clinically evident. A similar trend of Gb3 accumulation preceding clinical symptoms is observed in other organs, including the heart (*52*). In preclinical and clinical samples, Gb3 accumulation can be visualized and quantified using immunohistochemistry, thin-layer chromatography (TLC), electron microscopy, and mass spectroscopy (MS), being the last one the most quantitative and sensitive technique available.

The enhanced efficacy of nanoGLA, particularly in cardiac and renal tissues, and importantly in the brain, holds promise for addressing limitations observed with conventional ERT. The outcomes achieved with the nanoGLA formulation provides sufficient preclinical proof-of-concept data for the assumption that this nanoliposomal product containing GLA will be of substantial benefit to those patients affected by FD, and according to this, the EMA has granted to this product the orphan drug designation (ODD) (*21*). This designation underscores the potential clinical superiority of nanoGLA over authorized ERT, thereby validating the efficacy of this nanoencapsulation strategy and encouraging to advance this new therapeutic product toward clinical translation.

Therefore, an optimized nanoGLA production, combined with enhanced biodistribution and increased treatment efficacy, could allow for a reduced amount of API while achieving the same or improved therapeutic outcomes. This would result in a more cost-effective treatment. In addition, this gain in the efficacy could permit lowering the clinical dose and/or spacing the administration regimen for patients with Fabry disease. However, despite the important milestones achieved in this work, further studies must be carried out to determine the dose-response relationship and establish the appropriate dosing regimen showing efficacy, which will be crucial for a proper posology selection in preclinical species, and in patients with Fabry disease. Although the EE of the nanoGLA obtained by the DELOS process is high, the GLA loading capacity of the nanoliposomes without jeopardizing their physicochemical properties is limited. This is the reason why the nanovesicle concentration step by a TFF procedure was implemented to increase the GLA concentration in the formulation and enable in vivo dosing at therapeutic levels. In the present work, the applied concentration factor enabled performing in vivo efficacy studies at the GLA dose of 1 mg kg^{-1}. Subsequent investigations may involve adjusting this concentration factor after establishing the effective dose range for nanoGLA formulation.

Note that while the aqueous liquid dispersion represents the most advanced dosage form developed for the nanoGLA formulation, its EA stability is limited (≤3 months at 2° to 8°C). Consequently, a lyophilized-based product is being explored to enhance nanoGLA formulation stability.

Furthermore, regulatory toxicology studies are essential to assess the safety profile and define the therapeutic window of our nanomedicine to establish the optimal balance between efficacy and safety. NanoGLA is expected to reduce the immunogenicity against GLA. By encapsulating the GLA enzyme into the nanoliposomes, enzyme recognition (opsonization) is minimized, thereby reducing the generation of ADAs and the overall immune response. However, antibody measurement (ADA) will be conducted during repeated-dose toxicity studies. Antibody response will be characterized, and their appearance will be correlated with toxicological changes, according to *ICH S6 (R1): Preclinical safety evaluation of biotechnology-derived pharmaceuticals* (*30*). In addition, metabolomic analysis could provide insights into the complex interaction between the altered lipid metabolism in FD and how the liposomal components are processed. Collaboration with regulatory authorities will be continued to ensure compliance with relevant guidelines and standards. Through thorough investigation and adherence to regulatory requirements, we will be able to confidently progress toward clinical application of our nanomedicine, ultimately realizing its potential for improving patient outcomes.

MATERIALS AND METHODS

Materials

Cholesterol (chol; purity of 95%) was purchased from Panreac (Barcelona, Spain). 1,2-DPPC [molecular weight (MW) of 734.04, purity of 99%] was obtained from CordenPharma (Plankstadt, Germany). MKC (MW of 368.05, purity of 99.2%) was acquired from US Biological Life Science (Salem, USA). The cholesterol-PEG400-c(RGDfk) was specifically designed and synthesized by M. Royo's group from the Institut de Química Avançada de Catalunya (IQAC-CSIC, Barcelona, Spain) in the Synthesis of Peptide Unit (U3) of NANBIOSIS. The cyclic c-RGDfK peptide (simplified here as RGD) was synthesized and incorporated to a previously produced cholesterol-PEG400 intermediate, obtaining the cholesterol-PEG400-RGD, described as Chol-PEG8-RGD by E.C.-L. *et al.* (*53*). EtOH (HPLC grade, purity of ≥99.5%) was purchased from J.T.Baker (New Jersey, USA). DMSO (ACS reagent, purity of ≥99.9%) was obtained from Sigma-Aldrich (Madrid, Spain). CO_2 (purity of 99.9%) and nitrogen (N_2; purity of 99.9%) were supplied by Carburos Metálicos S.A. (Barcelona, Spain). The water was always pretreated with a Milli-Q Advantage A10 water purification system (Millipore Ibérica, Madrid, Spain). D-(+)-glucose (glucose, MW of 180.16, purity of ≥99.5%) was supplied from Sigma-Aldrich (Saint Louis, USA).

Production of rhGLA

The rhGLA was produced from a single batch at 50-liter scale in Leanbio SL facilities by mammalian cell culture using a stable clone of CHO cell line expressing a human α-galactosidase gene. This synthetic gene sequence was optimized for its expression in CHO cells and expresses the human GLA enzyme as described in UniProt entry P06280.

The broth culture was clarified by centrifugation and filtration followed by concentration step by TFF. A virus inactivation step introduced before chromatography purification. A series of two chromatography steps, anion exchange chromatography and hydrophobic interaction chromatography, was applied, and the eluate material was concentrated and diafiltrated using TFF. The product was formulated at same formulation buffer than commercial agalsidase beta formulation (Fabrazyme) and filtered by polyvinylidene difluoride (PVDF) (0.22 μm).

Production of intermediate nanoGLA (DELOS)

An EtOH:DMSO solution (4:1 volume ratio) containing DPPC (13.31 mg ml^{-1}), cholesterol (4.56 mg ml^{-1}), chol-PEG400-RGD (1.56 mg ml^{-1}), and MKC (0.64 mg ml^{-1}) was sonicated (10 min, 40°C) and loaded into a 50-ml high pressure vessel. The solution was

volumetrically expanded with liquid compressed CO_2 at a given CO_2 molar fraction (X_{CO2} = 0.45 to 0.55), working temperature (35°C), and pressure (8.5 MPa). The CO_2-expanded solution was kept 15 min under stirring (500 rpm) to achieve a complete homogenization. Then, a given volume of rhGLA stock solution (3.11 mg/ml, measured by RP-HPLC) was dissolved in purified water to reach the desired final rhGLA concentration (30 μg ml^{-1}). To form the nanoconjugates, the CO_2-expanded solution was depressurized into the aqueous solution containing the rhGLA. A N_2 flow (10 MPa) was used to plunge the CO_2-expanded solution from the reactor. In this way, intermediate nanoGLA batches were obtained [lipid (1.2 mg ml^{-1}), 5% (v/v) ethanol, and 1.25% (v/v) DMSO] and stored at 2° to 8°C.

Production of final nanoGLA (TFF)

Intermediate nanoGLA was submitted to a purification step based on TFF in aseptic-like conditions using a KrosFlo Research IIi TFF System (Repligen, Waltham, USA) placed inside a class II laminar flow biological safety cabinet (Maxisafe 2020, Thermo Fisher Scientific), following the procedures previously described in J.T.-M.'s thesis (*54*). All the material (tubes, reservoirs, and volumetric glass recipients) was sterilized by pressurized saturated steam autoclave (Presoclave-III 50, J.P.Selecta, 121°C, 20 min); plastic pieces (such as tubing connectors or reservoirs caps) were submerged overnight in ethanol. Hollow fiber columns (D04-E300-05-S) and pressure transductors were purchased directly in a sterile packaging (Repligen, USA). TFF system was set up following the manufacturer's recommendations. Hollow fiber columns were previously hydrated with water (2 ml cm^{-2}). Intermediate nanoGLA was concentrated 7.5-fold and diafiltrated six cycles in glucose solution [5% (w/v)], setting a certain feed flow (159 ml min^{-1}) and transmembrane pressure (5 to 10 TMP) during all the process, obtaining the final nanoGLA batches. All the process was done in cold conditions (ice-water bath) to preserve GLA activity. Obtained samples were stored at 2° to 8°C and always manipulated inside the laminar flow cabinet.

Determination of pH and osmolality

Samples were left at least 15 min at room temperature before determining pH (HI5221-02 pH meter, Hanna Instruments, USA). Values were expressed as the average of three measurements ± SD. No stirring was used to avoid sample disturbing.

Osmolality was measured using a freezing-point depression based osmometer (Osmomat-030, Gonotec, Germany) based on freezing-point determination, following the procedures previously described in J.T.-M.'s thesis (*54*). The equipment was calibrated at two points, zero adjustment (using pure water) and 300 mOsm kg^{-1} [using a standard calibration of physiological solution NaCl 0.9% (w/v) (Stada, Germany)]. Each solution (50 μl) was placed in a small 0.5-ml Eppendorf and introduced in the equipment for their measurement, ensuring that there were no visible air bubbles. Then, samples (50 μl) were measured under the same conditions. Reported values correspond to the average of three measurements ± SD.

Dynamic light scattering

Particle size distribution, PDI, and ζ-potential for nanoGLA were measured using a dynamic light scattering (DLS) and electrophoretic light scattering (ELS) analyzer combined with noninvasive backscatter technology (NIBS) (Malvern Zetasizer Nano ZS, Malvern Instruments, U.K), following procedures previously described in J.T.-M.'s thesis (*54*). The equipment was equipped with a 4 mW "red" He-Ne laser (λ = 632.8 nm) and with a thermostatic sample chamber. The detector was set at 173° for particle size distribution and 13° for ζ-potential measurements. Samples (1 ml) were placed in a disposable polystyrene cuvette (for DLS measurements) or in a disposable folded capillary cell (for ζ-potential measurements, applied voltage 40 mV). All samples were diluted in water if needed and analyzed at a concentration of 1.2 mg/ml. All reported values correspond to the average result of three consecutive measurements at 20°C on the same sample, recorded using the Zetasizer Software 7.13 (Malvern Panalytical, UK). Size data were based on intensity size distribution and correspond to *z* average (diameter) ± SD between the three measurements. The ζ-potential data were based on Smoluchowski model and correspond to ζ-potential average ± SD between the three measurements. For those samples that contain ethanol, solvent correction was applied to the values (ethanol, 0.8727 M). For stability studies, nanoGLA was stored at 2° to 8°C, and an aliquot was taken and analyzed at the established time points.

Cryo–transmission electron microscopy

Samples were equilibrated for 30 min at 25°C and then vitrified from this temperature in a controlled specimen preparation chamber following well-established procedures (*55*) and examined in a T12 G2 Tecnai (FEI) and a Talos F200C (Thermo Fisher Scientific) microscopes at cryogenic temperatures. Perforated Ted Pella grids were used; vitrified specimens' temperature was always kept below −170°C. Images were recorded with a Gatan UltraScan 2kx2k charge-coupled device camera or a Ceta camera at low dose operation, as previously described. No image processing was applied except for background subtraction.

Small-angle x-ray scattering

SAXS measurements were carried out at the instrument at Aarhus University. It is a NanoSTAR instrument (Bruker AXS) optimized for solution scattering with a liquid metal jet source (Excillum) and home-build scatterless slits (*56*). It is equipped with an automated sample handler, which injects 0.100 ml of the samples into a reusable quartz cell, in which both sample and background buffers were measured. The samples were measured without dilution. The data were background-subtracted and normalized to absolute scale using water as a standard employing programs from the SUPERSAXS package (*57*). The data were modeled (*24*, *25*) using a model of vesicles with a polydisperse overall size (fixed to 300 nm in diameter and a relative polydisperse of 25% due to limited low-*q* resolution of the experiment, where *q* is the modulus of the scattering vector the resolution of the experiment) with a bilayer cross section with a central Gaussians describing the low-electron density hydrocarbon moieties and two outer layers describing the more electron dense headgroup regions. Multilamellarity was described by a para-crystal model which included only single and double bilayers. The scattering from the alpha galactosidase dimer was used as a scalable background contribution for the samples containing the proteins. Because the PEG-RGD moieties give rise to a similar contribution to the scattering, the contribution from these were determined independently by measuring it for nonloaded samples, so that it could be taken into account in the modeling.

GLA concentration and EE

The rhGLA present in nanoGLA samples were analyzed in a RP-HPLC following the procedures previously described in J.T.-M.'s thesis (*54*) using an Infinity 1260 II HPLC system (Agilent

Technologies, USA), with a Zorbax 300SB-C18 (3.5 μm, 4.6 mm × 150 mm) column (Agilent Technologies, USA) at 60°C, and equipped with a ultraviolet detector (λ = 215 nm). NanoGLA was diluted in water to get an approximate rhGLA concentration of 20 to 30 μg/ml before its dispersion in an organic mixture, containing acetic acid (AcOH, 0.010 M, pH 5.5) and methanol (MeOH) in 1:1:1 volume (sample:AcOH:MeOH). Samples were prepared in replicates and injected into the equipment (100 μl, flow rate of 1 ml min^{-1}) after filtration (0.22-μm polytetrafluoroethylene). The mobile phase A consisted of 95% water, 5% acetonitrile, and 0.1% trifluoroacetic acid, and the mobile phase B consisted of 5% water, 95% acetonitrile, and 0.09% trifluoroacetic acid). Separation was done using a linear gradient from 0 to 60% of B (30 min) and cleaning step of 100% of B (5 min).

EE of rhGLA into liposomes was determined by comparing the amount of the enzyme encapsulated in the nanovesicles after removing the free GLA by diafiltration with the amount of initial GLA present in the raw batch obtained just after their production: EE% = (mass GLA after diafiltration/mass initial GLA) × 100.

Specific EA assay

GLA EA was assayed using fluorometric methods initially described by Desnick (*58*) with the modifications of Mayes *et al.* (*59*). The EA assay is based on the conversion of a nonfluorescent substrate [4-methylumbelliferyl α-D-galactopyranoside (4-MUG)] in a fluorescent product [4-methylumbelliferone (4-MU)] when active GLA is present. The protocol included the use of 4-MUG (M-7633 Sigma-Aldrich) as a substrate (2.46×10^{-3} M) in assay buffer [0.01 M acetic acid and 0.01 M acetate (pH 4.5)]. A typical assay reaction mixture contains 100 μl of 4-MUG and 25 μl of the sample. Enzymatic reactions took place in agitation (GLS Aqua 12 Plus, USA) at 25 rpm, 37°C for 1 hour. The reaction was stopped by glycine buffer (1.25 ml, 0.2 M, pH 10.4) and the released product (4-MU) was determined by fluorescence measurement (λ_{exc} = 365 nm, λ_{em} = 450 nm) using a microplate fluorescence reader (96 dark well plate, 200 μl per well, FLx800, Biotek, USA). Samples of commercial product 4-MU (Sigma-Aldrich) ranging from 5 to 500 ng ml^{-1} in glycine-NaOH buffer (0.2 M, pH 10.4) were used to obtain a calibration curve to transform fluorescence readings into product 4-MU concentration. Measurements were adjusted per time and protein quantity. Specific EA (expressed as μmol 4-MU mg^{-1} GLA $hour^{-1}$) was referred to EA of control reference GLA, agalsidase alfa (Replagal). Assays corresponded to a single representative experiment, replicated in three independent assays. For stability studies, nanoGLA was stored at 2° to 8°C, and an aliquot was taken and analyzed at the established time points.

Hemolysis test

For the hemolysis test, RBCs (isolated from WT mice) were resuspended in 2% (v/v) of PBS and exposed to different concentrations of test compounds during 1 hour at 37°C in duplicates. The amount of released hemoglobin was measured in a spectrophotometer at 405 nm (Biotek ELx800) after centrifugation (1000*g*, 10 min). Absorbance values were referred to a positive control of 100% hemolysis obtained after incubating RBC with 1% of Triton X-100. According to the manufacturer's protocol, samples showing hemolysis values below 5% can be considered nonhemolytic.

Plasma coagulation times

The effect of the nanoGLA in plasma coagulation was tested as previously reported (*60*) using the Start4 equipment (Stago, France) and following the manufacturer's protocol to determine the APTT, the PT, and the TT. Values were compared to the normal reference time ranges. Generally, prolongation ≥2-fold versus untreated control is considered physiologically significant. Testing samples (0.1 mg ml^{-1}) were incubated with human plasma (30 min, 37°C) in duplicates.

In vitro efficacy assays

MAECs from GLA-deficient mice (Gla^{tmKul1}) at passages 2 to 5 were seeded in 24-well plates. Twenty-four hours after seeding, 0.6 μM fluorescent *N*-dodecanoyl-NBD-ceramide trihexoside (NBD-Gb3, Matreya LCC) was added to the cultures along with specified concentrations of tested compounds. After 48-hour incubation, cells were trypsinized, and NBD-Gb3 fluorescent signal was analyzed by flow cytometry (FacsCalibur, Beckton Dickinson) and FCS Express v4 software. To calculate the percentage of NBD-Gb3 signal, fluorescent signal in control cells (without treatment) was established as 100%, and the values were accordingly normalized. The efficacy of GLA in reducing the Gb3 deposits was obtained as the percentage of Gb3 loss (i.e., % Gb3 loss = 100 − % Gb3-NBD signal).

Pharmacokinetic profile of empty liposomes

Animals

Protocols with rats used in this study were approved by the Austrian Ministry for Science and Research Ref.II/10b, Vienna. Male Sprague-Dawley rats with a weight of 400 to 800 g (Charles River Laboratories, Germany) were housed individually in acrylic glass cages with a 12-hour light/12-hour dark cycle, and food and water were available ad libitum.

Intravenous catheter surgery

Two days before dosing and sampling, animals were anesthetized by inhalation [% isoflurane in O_2 (1.9 liter $hour^{-1}$)] for placement of the intravenous catheter. The animals received one intravenous catheter into jugular vein. In addition, the animals were treated with the analgesic fentanyl (5 μg kg^{-1}, ip). After surgery, animals were transferred to awake-animal equipment (Raturn, BASi, USA) to recover from the surgery and to acclimatize to the equipment.

Dosing

Animals were connected to an awake-animal sampling system to allow assessment of blood sampling in conscious animals. Animals (n = 6 animals per group) were dosed intravenous with the testing compounds, empty liposomes (liposomes of 30 mg kg^{-1}; equivalent to MKC of 1 mg kg^{-1}), or free MKC at the equivalent concentration. Blood samples were taken according to sampling regimen.

Quantification of MKC in plasma by LC-MS

Procedures previously described in J.T.-M.'s thesis were followed (*54*). Briefly, plasma samples (10 μl) were diluted with an internal standard solution (ISTD) (10 μl) in CH_3CN (10 μl). As ISTD, a solution of cetyltrimethylammonium bromide (CTAB) (160 ng ml^{-1} in acetonitrile, CH3CN) was used, which is a compound that also belongs to the quaternary ammonium surfactant family. The mixture was vortexed and then centrifuged (5 min, 3000*g*). The supernatant was then analyzed by LC-MS. For calibration standards, a similar procedure was followed, diluting known amounts of MKC in buffer containing bovine serum albumin for obtaining a calibration curve in the range of 25 to 600 ng ml^{-1} for plasma samples. A solution of cetyltrimethylammonium bromide (CTAB) [160 ng ml^{-1} in acetonitrile (CH_3CN)] was used as internal standard solution, which is a compound that also belongs to the quaternary ammonium surfactant family. LC was performed using HPLC equipment (Vanquish,

Thermo Fisher Scientific), equipped with an Atlantis T3 (3 μm, 150 mm × 2.1 mm) column (Waters, USA) at 25°C. Injection sample volume was 4 μl, and the flow rate was 200 μl min^{-1}. The mobile phase A was composed by 0.3% of formic acid (HCOOH) in water, and the mobile phase B was composed by 0.3% of HCOOH in CH_3CN. Separation was done using a multistep gradient: 0.0 min (20% A, 80% B), 1.0 min (20% A, 80% B), 2.0 min (5% A, 95% B), 3.0 min (5% A, 95% B), 3.1 min (20% A, 80% B), and 5.1 min (20% A, 80% B). Approximate retention times were 3.2 and 3.6 min for MKC and CTAB, respectively. Next, MS was done using a triple quadrupole mass spectrometer equipment (TSQ Ultra AM, Thermo Fisher Scientific). The ionization method used positive electrospray ionization. Typical ionization parameters were the following: spray voltage of 3.0 kV, sheath gas of 15 AU, auxiliary gas of 5 AU, transfer capillary temperature of 320°C. The selected scan mode was SRM (selected reaction monitoring), which allows the selection of an ion of a particular mass in the first stage of the tandem MS and then is used as precursor of the second fragmentation reaction. For MKC (analyte), parent mass is 332.3 Da, product mass is 240.2 Da, and collision energy level is 18 eV. For CTAB (internal reference), parent mass is 284.3, product mass is 60.24 Da, and collision energy level is 28 eV. Detection parameters were the following: scan width of 0.4, scan time of 0.1, positive polarity, and peak width of 0.7.

Pharmacokinetic profile of nanoGLA

Animals and dosing

The study was performed in accordance with Labcorp Drug Development Standard Operating Procedures (Labcorp, UK) and following the procedures previously described in J.T.-M.'s thesis (*54*). Han Wistar healthy male rats (Charles River Laboratories, UK) with ages ranging from 63 to 70 days and target weight ranging from 210 to 290 g at dosing were kept in environmentally controlled rooms (19° to 25°C temperature, 40 to 70% relative humidity), and fluorescent light (nominal 12 hours) each day. All animals were allowed free access to main water from bottles attached to the cages. All procedures carried out on live animals as part of this study were subjected to provisions of United Kingdom National Law, particularly the Animals (Scientific Procedures) Act 1986. Male rats ($n = 3$ per group) were administered with the testing substances (free rhGLA or nanoGLA) at 1 mg kg^{-1} (GLA). Each animal received a single intravenous administration, as a bolus injection via a lateral tail vein, at a nominal dose volume of 0.32 ml kg^{-1} for rhGLA or 3.7 ml kg^{-1} for nanoGLA. Serial blood samples (300 μl) were collected from all the animals at eight time points (0.016-, 0.16-, 0.5-, 1-, 2-, 4, 6-, and 8-hour post-dose) by venepuncture from the jugular vein, except for the final sample that was collected by cardiac puncture while under terminal inhalation anesthesia (isoflurane in oxygen). All animals were observed at the beginning and the end of the working day and at each blood sampling occasion for any abnormal signs. Blood was collected into tubes containing K2-EDTA (ethylenediaminetetraacetic acid) anticoagulant and centrifuged (800*g*, 10 min, 4°C) to produce plasma for analysis, and residual blood cells were discarded. The resultant plasma samples were split into two aliquots of approximately equal volume. Samples were processed to plasma within 30 min of collection and snap-frozen on dry ice within 60 min (<−50°C).

Quantification of GLA in plasma by ELISA

The amount of rhGLA present in rat plasma was quantified by an enzyme-linked immunosorbent assay (ELISA) method performed by Labcorp Drug Development (UK) and Unilabs York Bioanalytical Solutions (UK) (*54*). Briefly, mouse anti-GLA antibodies solution (mouse polyclonal antibody to GLA, reference no. 169315, Abcam, UK) was added into a 96-well immunoplate (50 μl per well; Nunc MaxiSorp, Thermo Fisher Scientific) and incubated for 14 to 24 hours at 4°C. After washing [3×, 300 μl per well of PBS solution containing 0.05% (v/v) Tween 20], the plate was blocked (200 μl) using SuperBlock (reference no. 37515, Thermo Fisher Scientific, USA) for 1 to 2 hours. After another wash step (3×, 300 μl), plasma samples diluted 1.5 in buffer (low cross buffer, reference no. 100500, Candor Biosciences) containing Triton X-100 (2% w/v) were then added to the plate and incubated for 1 hour. The use of Triton X-100 was required to disrupt the nanoliposomes and allow GLA release for quantification. After a further wash step, sheep anti-GLA antibodies solution (sheep polyclonal antibody to GLA, reference no. AF6146, R&D Systems, USA) was added to the plate (50 μl per well) and incubated for 1 hour. After a further wash step, anti-sheep peroxidase conjugate solution (anti-sheep immunoglobulin G peroxidase, reference no. A3415, Sigma-Aldrich, USA) was added to the plate (50 μl per well) and incubated for 1 hour. After a final wash step, a trimethylboron substrate (reference no. T4444, Sigma-Aldrich, USA) was added (50 μl per well). Reaction was stopped after 20 min, adding the stop solution (0.5 M, sulfuric acid, reference no. 07208, Sigma-Aldrich). Absorbance was read within 15 min of the reaction being stopped in a suitable plate reader (Tecan Infinite 200 Pro), at $\lambda_{Abs} = 450$ nm with a reference $\lambda_{Ref} = 620$ nm. Besides, calibration standards were also prepared in rat plasma using known amounts of rhGLA and following the same protocol.

In vivo biodistribution and efficacy studies in Fabry mouse model

All animal experimentation using Fabry mice, including the obtention of MAEC, was performed following procedures previously approved by the Ethical Committee for the Use of Experimental Animals at the Vall d'Hebron Research Institute, Barcelona and the local government (CEA-OH/9572). Monitoring of the animals included the close recording of any signs of distress, toxicity, or abnormal physical conditions that could be related to the administration of nanoGLA, rhGLA or agalsidase alfa. These biodistribution and efficacy assays were performed by the ICTS "NANBIOSIS" at the CIBERBBN's Functional Validation and Preclinical Research (FVPR)/U20 (www.nanbiosis.es/portfolio/u20-in-vivo-experimental-platform/; Barcelona, Spain) using male GLA-deficient mice (Gla^{tmKul1}, C57BL/6 background) with ages ranging from 2 to 4 months. Once completed, blood and tissues samples were collected and stored at −80°C upon analysis.

In biodistribution assays, Fabry KO mice ($n = 8$ per group) were treated by tail vein injection with total GLA protein (1 mg kg^{-1}), following the procedures previously described in J.T.-M.'s thesis (*54*). Treatment groups included nanoGLA and free enzymes (rhGLA and agalsidase alfa -Replagal). WT and KO mice without GLA treatment were also included as controls. In each treatment group, half of the animals were euthanized 1 min after administration and the other half 30 min after administration. GLA EA was measured in harvested tissues, following procedures described above, a referred to the total protein content determined by the bicinchoninic acid (BCA) method (Pierce, Thermo Fisher Scientific). Last, EA values at 30 min were referred to those in plasma 1 min after administration and expressed as % of injected dose (ID).

For single-dose efficacy assays, Fabry KO mice ($n = 24$) were randomized by age in four different groups [nanoGLA, rhGLA, agalsidase alfa (Replagal), and vehicle] and received a single dose of GLA protein

($1\ mg\ kg^{-1}$) and were euthanized 1 week after treatment (*54*). Repeated dose efficacy assays used the same number of animals and group distribution. In this later assay, animals received eight doses of $1\ mg\ kg^{-1}$ every other day and were euthanized 24 hours after the last administration. Vehicle treated animals receive the corresponding volume of PBS, and additional group of nontreated WT male littermates was also included in both experiments. In the absence of any record of side-effect or weight loss in the animals, we concluded that the treatment was well-tolerated in the tested dose range.

Gb3 and LysoGb3 levels were determined with LC-HRMS at the Institute of Advanced Chemistry of Catalonia (IQAC-CSIC). In detail, 750 µl of a methanol-chloroform (2:1, v/v) solution containing internal standards (*N*-dodecanoylsphingosine, *N*-dodecanoylglucosylsphingosine, *N*-dodecanoylsphingosylphosphorylcholine, and *N*-heptadecanoylceramide trihexoside; 0.2 nmol each) were added to the plasma (0.1 ml) or tissue homogenates (0.1 ml, protein around 0.3 mg/ml). Samples were extracted at 48°C overnight and cooled, 75 µl of 1 M KOH in methanol was added, and the mixture was incubated for 2 hours at 37°C. Following the addition of 75 µl of 1 M acetic acid, samples were evaporated to dryness and stored at −20°C until the analysis of sphingolipids. Before the analysis, 150 µl of methanol was added to the samples and centrifuged at 13,000*g* for 5 min, and 130 µl of the supernatant was transferred to a new vial and injected. Sphingolipids were measured with an Acquity ultraperformance LC (UPLC) system connected to a time-of-flight (TOF) (LCT Premier XE) detector controlled with Waters/Micromass MassLynx software. Sample was injected onto an UPLC BEH C8 column (particle size, 1.7 µm; 100 mm by 2.1 mm); flow rate of $0.3\ ml\ min^{-1}$ and column temperature of 30°C were used. The mobile phase was methanol with 1 mM ammonium formate and 0.2% formic acid (solution A) and water with 2 mM ammonium formate and 0.2% formic acid (solution B). Gradient elution started at 80% solution A was increased to 90% solution A over 3 min, held for 3 min, increased to 99% solution A over 9 min, and then held for 3 min. Initial conditions were attained for 2 min, and the system was stabilized for 3 min. The acquisition range of the TOF detector was mass/charge ratio 50 to 1500, the capillary voltage was set to 3.0 kV, the desolvation temperature was 350°C, and the desolvation gas flow rate was $600\ liter\ hour^{-1}$. Quantification was carried out using the ion chromatogram obtained for each compound using 50-mDa windows. The linear dynamic range was determined by injection of standard mixtures. Positive identification of compounds was based on accurate mass measurements with an error <5 parts per million and LC retention time compared to that of a standard (<2%). Quantification of was carried out against internal standard (*N*-heptadecanoylceramide trihexoside), whereas lysoGb3 was quantified using external standard calibration.

Results for in vivo efficacy assays were expressed as % Gb3 loss. For calculation of the relative Gb3 loss, it was assumed that the difference in Gb3 levels between nontreated KO mice and WT counterparts corresponds to a 100% of Gb3 loss in WT. Then, the Gb3 levels in different treatment groups were referred to this total Gb3 loss in WT, meaning that those treatments with a higher percentage of Gb3 loss are the ones with a higher efficacy.

Supplementary Materials

This PDF file includes:

Figs. S1 to S8

Tables S1 to S7

REFERENCES AND NOTES

1. Y. A. Zarate, R. J. Hopkin, Fabry's disease. *Lancet* **372**, 1427–1435 (2008).
2. C. Carnicer-Cáceres, J. A. Arranz-Amo, C. Cea-Arestin, M. Camprodon-Gomez, D. Moreno-Martinez, S. Lucas-Del-pozo, M. Moltó-Abad, A. Tigri-Santiña, I. Agraz-Pamplona, J. F. Rodriguez-Palomares, J. Hernández-Vara, M. Armengol-Bellapart, M. Del-Toro-riera, G. Pintos-Morell, Biomarkers in fabry disease. Implications for clinical diagnosis and follow-up. *J. Clin. Med.* **10**, 1664 (2021).
3. P. F. Bodary, J. A. Shayman, D. T. Eitzman, α-Galactosidase A in Vascular Disease. *Trends Cardiovasc. Med.* **17**, 129–133 (2007).
4. J. S. Shen, X. L. Meng, D. F. Moore, J. M. Quirk, J. A. Shayman, R. Schiffmann, C. R. Kaneski, Globotriaosylceramide induces oxidative stress and up-regulates cell adhesion molecule expression in Fabry disease endothelial cells. *Mol. Genet. Metab.* **95**, 163–168 (2008).
5. K. Kok, K. C. Zwiers, R. G. Boot, H. S. Overkleeft, J. M. F. G. Aerts, M. Artola, Fabry disease: Molecular basis, pathophysiology, diagnostics and potential therapeutic directions. *Biomolecules* **11**, 271 (2021).
6. A. F. Leal, A. J. Espejo-Mojica, O. F. Sánchez, C. M. Ramírez, L. H. Reyes, J. C. Cruz, C. J. Alméciga-Díaz, Lysosomal storage diseases: Current therapies and future alternatives. *J. Mol. Med.* **98**, 931–946 (2020).
7. Agency European Medicines, Fabrazyme (European Medicines Agency, EMEA/H/C/000370 - II/0116, 2020); www.ema.europa.eu/en/medicines/human/EPAR/fabrazyme.
8. D. P. Germain, Fabry disease. *Orphanet J Rare Dis* **5**, 30 (2010).
9. F. C. Fervenza, R. Torra, D. G. Warnock, Safety and efficacy of enzyme replacement therapy in the nephropathy of fabry disease. *Biol. Targets Ther.* **2**, 823–843 (2008).
10. C. Siatskas, J. A. Medin, Gene therapy for fabry disease. *J. Inherit. Metab. Dis.* **24**, 25 (2001).
11. R. Schiffmann, O. Goker-Alpan, M. Holida, P. Giraldo, L. Barisoni, R. B. Colvin, C. J. Jennette, G. Maegawa, S. A. Boyadjiev, D. Gonzalez, K. Nicholls, A. Tuffaha, M. G. Atta, B. Rup, M. R. Charney, A. Paz, M. Szlaifer, S. Alon, E. Brill-Almon, R. Chertkoof, D. Hughes, Pegunigalsidase alfa, a novel PEGylated enzyme replacement therapy for fabry disease, provides sustained plasma concentrations and favorable pharmacodynamics: A 1-year phase 1/2 clinical Trial. *J. Inherit. Metab. Dis.* **42**, 534–544 (2019).
12. J. J. Miller, A. J. Kanack, N. M. Dahms, Progress in the understanding and treatment of Fabry disease. *Biochim. Biophys. Acta Gen. Subj.* **1864**, 129437 (2020).
13. A. Felis, M. Whitlow, A. Kraus, D. G. Warnock, E. Wallace, Current and investigational therapeutics for fabry disease. *Kidney Int. Rep.* **5**, 407–413 (2020).
14. Agency European Medicines, Galafold (European Medicines Agency, MEA/H/C/004059 - II/0038, 2023); www.ema.europa.eu/en/medicines/human/EPAR/galafold.
15. O. Azevedo, M. F. Gago, G. Miltenberger-Miltenyi, N. Sousa, D. Cunha, Fabry disease therapy: State-of-the-art and current challenges. *Int. J. Mol. Sci.* **22**, 206 (2020).
16. I. Abasolo, J. Seras-Franzoso, M. Moltó-Abad, V. Díaz-Riascos, J. L. Corchero, G. Pintos-Morell, S. Schwartz, Nanotechnology-based approaches for treating lysosomal storage disorders, a focus on fabry disease. *Wiley Interdiscip. Rev. Nanomed. Nanobiotechnol.* **13**, e1684 (2021).
17. S. Muro, Strategies for delivery of therapeutics into the central nervous system for treatment of lysosomal storage disorders. *Drug Deliv. Transl. Res.* **2**, 169–186 (2012).
18. M. Jeyakumar, R. A. Dwek, T. D. Butters, F. M. Platt, Storage solutions: Treating lysosomal disorders of the brain. *Nat. Rev. Neurosci.* **6**, 713–725 (2005).
19. A. K. A. Silva, C. Sagné, F. Gazeau, I. Abasolo, Enzyme replacement therapy: current challenges and drug delivery prospects via extracellular vesicles. *Rare Dis. Orphan Drugs J.* **1**, 13 (2022).
20. N. Ventosa, J. Veciana, M. Royo, J. Tomsen-Melero, I. Abasolo, S. Schwartz, J. L. Corchero Nieto, D. Pulido, E. Cristóbal-Lecina, E. González-Mira, S. Sala Vergés, A. Cordoba, J. Merlo-Mas, A. Soldevila, A. Font, Liposomes and its use for enzyme delivery, WO 2022/161990 A1, World Intellectual Property Organization (2022).
21. European Commission, Community Register of orphan medicinal products (Designation number: EU/3/20/2396*EU/3/20/2396*, 2021); https://ec.europa.eu/health/documents/community-register/html/o2396.htm.
22. J. Sambrook, in *Molecular Cloning a Laboratory Manual* (Cold Spring Harbor Laboratory Press, 2001), pp. 16.1–16.54.
23. I. Cabrera, I. Abasolo, J. L. Corchero, E. Elizondo, P. R. Gil, E. Moreno, J. Faraudo, S. Sala, D. Bueno, E. González-Mira, M. Rivas, M. Melgarejo, D. Pulido, F. Albericio, M. Royo, A. Villaverde, M. F. García-Parajo, S. Schwartz Jr., N. Ventosa, J. Veciana, α-Galactosidase-a loaded-nanoliposomes with enhanced enzymatic activity and intracellular penetration. *Adv. Healthc. Mater.* **5**, 829–840 (2016).
24. J. Tomsen-Melero, S. Passemard, N. García-Aranda, Z. V. Díaz-Riascos, R. González-Rioja, J. Nedergaard Pedersen, J. Lyngsø, J. Merlo-Mas, E. Cristóbal-Lecina, J. L. Corchero, D. Pulido, P. Cámara-Sánchez, I. Portnaya, I. Ionita, S. Schwartz Jr., J. Veciana, S. Sala, M. Royo, A. Córdoba, D. Danino, J. S. Pedersen, E. González-Mira, I. Abasolo, N. Ventosa, Impact of chemical composition on the nanostructure and biological activity of α-Galactosidase-loaded nanovesicles for fabry disease treatment. *ACS Appl. Mater. Interfaces* **13**, 7825–7838 (2021).
25. J. Merlo-Mas, J. Tomsen-Melero, J.-L. Corchero, E. González-Mira, A. Font, J. N. Pedersen, N. García-Aranda, E. Cristóbal-Lecina, M. Alcaina-Hernando, R. Mendoza, E. Garcia-Fruitós, T. Lizarraga, S. Resch, C. Schimpel, A. Falk, D. Pulido, M. Royo, S. Schwartz Jr., I. Abasolo,

J. S. Pedersen, D. Danino, A. Soldevila, J. Veciana, S. Sala, N. Ventosa, A. Córdoba, Application of quality by design to the robust preparation of a liposomal GLA formulation by DELOS-susp method. *J. Supercrit. Fluids* **173**, 105204 (2021).
26. F. Khan, P. M. Legler, R. M. Mease, E. H. Duncan, E. S. Bergmann-Leitner, E. Angov, Histidine affinity tags affect MSP1(42) structural stability and immunodominance in mice. *Biotechnol. J.* **7**, 133–147 (2012).
27. U. Bulbake, S. Doppalapudi, N. Kommineni, W. Khan, Liposomal formulations in clinical use: An updated review. *Pharmaceutics* **9**, 12 (2017).
28. E. Beltrán-Gracia, A. López-Camacho, I. Higuera-Ciapara, J. B. Velázquez-Fernández, A. A. Vallejo-Cardona, *Nanomedicine review: Clinical developments in liposomal applications* (Springer, 2019); https://doi.org/10.1186/s12645-019-0055-y.
29. J. Seras-Franzoso, Z. V. Díaz-Riascos, J. L. Corchero, P. González, N. García-Aranda, M. Mandaña, R. Riera, A. Boullosa, S. Mancilla, A. Grayston, M. Moltó-Abad, E. Garcia-Fruitós, R. Mendoza, G. Pintos-Morell, L. Albertazzi, A. Rosell, J. Casas, A. Villaverde, S. Schwartz Jr., I. Abasolo, Extracellular vesicles from recombinant cell factories improve the activity and efficacy of enzymes defective in lysosomal storage disorders. *J. Extracell. Vesicles* **10**, e12058 (2021).
30. European Medicine Agency, ICH guideline S6 (R1) on preclinical safety evaluation of biotechnology-derived pharmaceuticals (EMA/CHMP/ICH, 2011), pp. 1–22.
31. G. M. Raj, in *Introduction to Basics of Pharmacology and Toxicology*, G. M. Raj, R. Raveendran, Eds. (Springer, 2019).
32. P. M. Glassman, V. R. Muzykantov, Pharmacokinetic and pharmacodynamic properties of drug delivery systems. *J. Pharmacol. Exp. Ther.* **370**, 570–580 (2019).
33. T. Ohshima, G. J. Murray, W. D. Swaim, G. Longenecker, J. M. Quirk, C. O. Cardarelli, Y. Sugimoto, I. Pastan, M. M. Gottesman, R. O. Brady, A. B. Kulkarni, α-Galactosidase a deficient mice: A model of fabry disease. *Proc. Natl. Acad. Sci. U.S.A.* **94**, 2540–2544 (1997).
34. K. Lee, X. Jin, K. Zhang, L. Copertino, L. Andrews, J. Baker-Malcolm, L. Geagan, H. Qiu, K. Seiger, D. Barngrover, J. M. McPherson, T. Edmunds, A biochemical and pharmacological comparison of enzyme replacement therapies for the glycolipid storage disorder Fabry disease. *Glycobiology* **13**, 305–313 (2003).
35. J. Tomsen-Melero, J. Merlo-Mas, A. Carreño, S. Sala, A. Córdoba, J. Veciana, E. González-Mira, N. Ventosa, Liposomal formulations for treating lysosomal storage disorders. *Adv. Drug Deliv. Rev.* **190**, 114531 (2022).
36. L. Ferrer-Tasies, H. Santana, I. Cabrera-Puig, E. González-Mira, L. Ballell-Hosa, C. Castellar-Álvarez, A. Cordoba, J. Merlo-Mas, H. Gerónimo, G. Chinea, V. Falcón, E. Moreno-Calvo, J. S. Pedersen, J. Romero, C. Navarro-Requena, C. Valdés, M. Limonta, J. Berlanga, S. Sala, E. Martínez, J. Veciana, N. Ventosa, Recombinant human epidermal growth factor/quatsome nanoconjugates: A robust topical delivery system for complex wound healing. *Adv. Ther.* **4**, 2000260 (2021).
37. Y. A. Ioannou, K. M. Zeidner, R. E. Gordon, R. J. Desnick, Fabry disease: Preclinical studies demonstrate the effectiveness of α-galactosidase a replacement in enzyme-deficient mice. *Am. J. Hum. Genet.* **68**, 14–25 (2001).
38. T. Kizhner, Y. Azulay, M. Hainrichson, Y. Tekoah, G. Arvatz, A. Shulman, I. Ruderfer, D. Aviezer, Y. Shaaltiel, Characterization of a chemically modified plant cell culture expressed human α-Galactosidase-A enzyme for treatment of Fabry disease. *Mol. Genet. Metab.* **114**, 259–267 (2015).
39. T. Kodama, T. Tsukimura, I. Kawashima, A. Sato, H. Sakuraba, T. Togawa, Differences in cleavage of globotriaosylceramide and its derivatives accumulated in organs of young Fabry mice following enzyme replacement therapy. *Mol. Genet. Metab.* **120**, 116–120 (2017).
40. J. S. Shen, A. Busch, T. S. Day, X. L. Meng, C. I. Yu, P. Dabrowska-Schlepp, B. Fode, H. Niederkrüger, S. Forni, S. Chen, R. Schiffmann, T. Frischmuth, A. Schaaf, Mannose receptor-mediated delivery of moss-made α-galactosidase a efficiently corrects enzyme deficiency in Fabry mice. *J. Inherit. Metab. Dis.* **39**, 293–303 (2016).
41. W. Tian, Z. Ye, S. Wang, M. A. Schulz, J. Van Coillie, L. Sun, Y.-H. Chen, Y. Narimatsu, L. Hansen, C. Kristensen, U. Mandel, E. P. Bennett, S. Jabbarzadeh-Tabrizi, R. Schiffmann, J.-S. Shen, S. Y. Vakhrushev, H. Clausen, Z. Yang, The glycosylation design space for recombinant lysosomal replacement enzymes produced in CHO cells. *Nat. Commun.* **10**, 1785 (2019).
42. T. Togawa, T. Kodama, T. Suzuki, K. Sugawara, T. Tsukimura, T. Ohashi, N. Ishige, K. Suzuki, T. Kitagawa, H. Sakuraba, Plasma globotriaosylsphingosine as a biomarker of Fabry disease. *Mol. Genet. Metab.* **100**, 257–261 (2010).
43. W. Wang, Tolerability of hypertonic injectables. *Int. J. Pharm.* **490**, 308–315 (2015).
44. S. D. Carstairs, J. R. Suchard, T. Smith, L. V. Simon, C. J. Kalynych, M. Shimada, D. A. Tanen, Contribution of serum ethanol concentration to the osmol gap: A prospective volunteer study. *Clin. Toxicol.* **51**, 398–401 (2013).
45. J. R. Oster, I. Singer, Hyponatremia, hyposmolality, and hypotonicity: Tables and fables. *Arch. Intern. Med.* **159**, 333–336 (1999).
46. Gilead Sciences, AmBisome (amphotericin B) liposome for injection (2020); www.gilead.com/-/media/files/pdfs/medicines/other/ambisome/ambisome_pi.pdf.
47. Health Products Regulatory Authority, DaunoXome–Summary of Product Characteristics (2014); www.hpra.ie/img/uploaded/swedocuments/LicenseSPC_PA1329-009-001_11082014151041.pdf.
48. Baxter Healthcare Corporation, DOXIL–Prescribing Information (2019); www.baxterpi.com/pi-pdf/Doxil_Baxter_PI.pdf.
49. European Medicines Agency, Caelyx–Summary of product characteristics (2006); www.ema.europa.eu/en/documents/product-information/caelyx-pegylated-liposomal-epar-product-information_en.pdf.
50. Neon Healthcare Ltd, Visudyne–Package leaflet: Information for the user (2022); www.medicines.org.uk/emc/files/pil.14186.pdf.
51. B. Najafian, E. Svarstad, L. Bostad, M. C. Gubler, C. Tøndel, C. Whitley, M. Mauer, Progressive podocyte injury and globotriaosylceramide (GL-3) accumulation in young patients with Fabry disease. *Kidney Int.* **79**, 663–670 (2011).
52. M. J. Hsu, F. P. Chang, Y. H. Lu, S. C. Hung, Y. C. Wang, A. H. Yang, H. J. Lee, S. H. Sung, Y. F. Wang, W. C. Yu, T. R. Hsu, P. H. Huang, S. K. Chang, I. Dzhagalov, C. L. Hsu, D. M. Niu, Identification of lysosomal and extralysosomal globotriaosylceramide (Gb3) accumulations before the occurrence of typical pathological changes in the endomyocardial biopsies of Fabry disease patients. *Genet. Med.* **21**, 224–232 (2019).
53. E. Cristóbal-Lecina, D. Pulido, P. Martin-Malpartida, M. J. Macias, F. Albericio, M. Royo, Synthesis of stable cholesteryl-polyethylene glycol-peptide conjugates with non-disperse polyethylene glycol lengths. *ACS Omega* **5**, 5508–5519 (2020).
54. J. Tomsen Melero, thesis, Universitat Autònoma de Barcelona (2021).
55. D. Danino, Cryo-TEM of Soft Molecular Assemblies. *Curr. Opin. Colloid Interface Sci.* **17**, 316–329 (2012).
56. J. Lyngsø, J. S. Pedersen, A high-flux automated laboratory small-angle X-ray scattering instrument optimized for solution scattering. *J. Appl. Crystallogr.* **54**, 295–305 (2021).
57. C. L. P. Oliveira, T. Vorup-Jensen, C. Andersen, G. Andersen, J. Pedersen, Discovering new features of protein complexes structures by small-angle x-ray scattering, in *Applications of Synchrotron Light to Scattering and Diifraction in Materials and Life Sciences* (Springer, 2009), pp. 231–244.
58. R. J. Desnick, Fabry's disease: Enzymatic diagnosis of hemizygotes and heterozygotes. *J. Lab. Clin. Med.* **81**, 157–171 (1973).
59. J. S. Mayes, J. B. Scheerer, R. N. Sifers, M. L. Donaldson, Differential assay for lysosomal alpha-galactosidases in human tissues and its application to fabry's disease. *Clin. Chim. Acta* **112**, 247–251 (1981).
60. D. Rafael, F. Martínez, F. Andrade, J. Seras-Franzoso, N. Garcia-Aranda, P. Gener, J. Sayós, D. Arango, I. Abasolo, S. Schwartz Jr., Efficient EFGR mediated siRNA delivery to breast cancer cells by cetuximab functionalized Pluronic® F127/Gelatin. *Chem. Eng. J.* **340**, 81–93 (2018).

Acknowledgments: This research was supported by CIBER–Consorcio Centro de Investigación Biomédica en Red (groups CB06/01/0033, CB06/01/0074, CB06/01/0014, and CB06/01/0012), Instituto de Salud Carlos III, Ministerio de Ciencia e Innovación. Part of this work has been done in the framework of the J.T.-M.' thesis in Materials Science of the Universitat Autònoma de Barcelona and in the frame of M.M.-A.'s thesis in the Biochemistry, Molecular Biology and Biomedicine doctoral program of the UAB. We acknowledgment the ICTS NANBIOSIS for the support of the Synthesis of Peptide Unit (U3), Biomaterial Processing and Nanostructuring Unit (U6), and In vivo experimentation unit (FPVR/U20). We acknowledge the support of the Servei de Microscopia from the Universitat Autònoma de Barcelona (UAB) and thank M. de Cabo for the professional assistance with cryo-TEM and P. Tudela from the Department de Biologia cellular, de fisiologia i de immunologia from the UAB for the assistance with the osmometer. **Funding:** This work was supported by the European Union's Horizon 2020 research and innovation programme under grant agreement no. 720942 (SMART4FABRY); the European Union's Horizon 2020 research and innovation programme 953110 PHOENIX-OITB (to J.T.-M., J.M.-M., A.S., A.Ca., A.F., S.Sa., A.Có., N.V., and E.G.-M.); European Union EIC Transition, 101136772 Nano4Rare (to J.T.-M., A.Ca., N.V., and E.G.-M.); the Generalitat de Catalunya, FI-AGAUR, Secretary of Universities and Research of the Department of Business and Knowledge of the Generalitat de Catalunya and the European Social Fund (ESF–Investing in your future) of the European Union (to J.T.-M.); CIBER-BBN, EXPLORE-3, and PEGLyso-2 project (to I.A.); the Instituto de Salud Carlos III grants PI18/00871 and PI21/00936, cofounded by European Regional Development Fund (to I.A.); Catalan Government's Strategic Plan for Research and Innovation in Health, PERIS, SLT01720000181 (to M.M.-A.); the Generalitat de Catalunya, 2017 SGR 1439 and 2021 SGR 00230 (to E.C.-L., D.P., and M.R.), 2021 SGR 1173 (to I.A.), and 2021 SGR 00438 (to J.T.-M., A.Ca., J.V., N.V., and E.G.-M.); Generalitat de Catalunya, AGAUR, 2021 INNOV 00053 (to J.T.-M., A.Ca., N.V., and E.G.-M.); the Ministerio de Ciencia e Innovación, Plan Estatal de Investigación Científica y Técnica y de Innovación (PEICTI) 2021–2023, PID2022-137332OB-I00 (ARMONIA) (to J.T.-M., A.Ca., N.V., and E.G.-M.); and the Ministerio de Ciencia e Innovación, Severo Ochoa Programme, CEX2019-000917-S (FUNFUTURE) and CEX2023-001263-S (to J.T.-M., A.Ca., N.V., and E.G.-M.). **Author contributions:** Conceptualization: J.T.-M., J.M.-M., Z.V.D.-R., A.Có., N.V., I.A., and E.G.-M. Methodology: J.T.-M., M.M.-A., J.M.-M., Z.V.D.-R., E.C.-L., A.S., T.A.-K., I.I., J.S.P., H.C., J.L.C., D.P., J.C., A.F., T.B., A.Có., I.A., and E.G.-M. Investigation: J.T.-M., M.M.-A., J.M.-M., Z.V.D.-R., E.C.-L., T.A.-K., J.S.P., A.Ca., J.L.C., A.F., and M.R. Visualization: J.T.-M., I.A., and E.G.-M. Funding acquisition: A.S., D.D., S.K.P., L.S., H.C., J.L.C., J.V., S.Sa., T.B., M.R., A.Có., N.V., I.A., and E.G.-M. Project administration: N.V. and E.G.-M. Supervision: A.S., H.C., T.B., A.Có., N.V., I.A., and E.G.-M. Writing—original draft: J.T.-M., I.A., and E.G.-M. Writing—review and editing: J.T.-M., M.M.-A., J.M.-M., Z.V.D.-R., E.C.-L., A.S., T.A.-K., D.D., J.S.P., H.C., J.L.C., D.P., J.V., M.R., A.Có., N.V., I.A., and E.G.-M. **Competing interests:** The authors declare the following financial interests/personal relationships which may be

considered as potential competing interests: D.P., S.Sc., M.R., I.A., S.Sa., J.L.C., J.V., and N.V. are the inventors of patent WO/2014/001509. S.Sa., J.V., and N.V. are inventors of patent WO/2006/079889 owned by Nanomol Technologies SL and are stockholders in Nanomol Technologies SL. J.T.-M., J.M.-M., S.Sa., A.Có., J.L.C., I.A., S.Sc., A.S., A.F., E.C.-L., M.R., D.P., J.V., N.V., and E.G.-M. are the inventors of patent application no. WO 2022/161990 A1. All other authors declare that they have no competing interests. **Data and materials availability:** All data needed to evaluate the conclusions in the paper are present in the paper and/or the Supplementary Materials. The use of the HMEC-1 cells and Fabry KO mice was possible thanks to the signature of two MTAs with the Center of Disease Control (CDC, USA) and the Jackson Laboratory (as repository of transgenic mice originally produced in A. Kulkarni's laboratory in the NIH), respectively.

Submitted 15 May 2024
Accepted 7 November 2024
Published 13 December 2024
10.1126/sciadv.adq4738